Atmos. Chem. Phys. Discuss., 13, 1979–2034, 2013
www.atmos-chem-phys-discuss.net/13/1979/2013/
doi:10.5194/acpd-13-1979-2013

Atmospheric Chemistry and Physics Discussions

Observations of gas- and aerosol-phase organic nitrates at BEACHON-RoMBAS 2011

J. L. Fry[1], D. C. Draper[1], K. J. Zarzana[2,3], P. Campuzano-Jost[2,3], D. A. Day[2,3], J. L. Jimenez[2,3], S. S. Brown[4], R. C. Cohen[5], L. Kaser[6], A. Hansel[6], L. Cappellin[7], T. Karl[8], A. Hodzic Roux[8], A. Turnipseed[8], C. Cantrell[8], B. L. Lefer[9], and N. Grossberg[9]

[1]Department of Chemistry, Reed College, Portland, OR, USA
[2]Department of Chemistry and Biochemistry, University of Colorado Boulder, Boulder, CO, USA
[3]Cooperative Institute for Research in Environmental Sciences (CIRES), Boulder, CO, USA
[4]Earth System Research Laboratory, National Oceanic and Atmospheric Administration, Boulder, CO, USA
[5]Department of Chemistry, University of California at Berkeley, Berkeley, CA, USA
[6]Institute for Ion Physics and Applied Physics, University of Innsbruck, Innsbruck, Austria
[7]IASMA Research and Innovation Centre, Fondazione Edmund Mach, Food Quality and Nutrition Area, S. Michele a/A, Italy
[8]Atmospheric Chemistry Division, National Center for Atmospheric Research, Boulder, CO, USA

[9]Department of Earth and Atmospheric Science, University of Houston, Houston, TX, USA

Received: 23 October 2012 – Accepted: 30 December 2012 – Published: 21 January 2013

Correspondence to: J. L. Fry (fry@reed.edu)

Published by Copernicus Publications on behalf of the European Geosciences Union.

Abstract

At the Rocky Mountain Biogenic Aerosol Study (BEACHON-RoMBAS) field campaign in the Colorado front range, July–August 2011, measurements of gas- and aerosol-phase organic nitrates enabled a study of the role of NO_x ($NO_x = NO + NO_2$) in oxidation of forest-emitted VOCs and subsequent aerosol formation. Substantial formation of peroxy- and alkyl-nitrates is observed every morning, with an apparent 2.9 % yield of alkyl nitrates from daytime RO_2 + NO reactions. *Aerosol-phase* organic nitrates, however, peak in concentration during the night, with concentrations up to 140 ppt as measured by both optical spectroscopic and mass spectrometric instruments. The diurnal cycle in aerosol fraction of organic nitrates shows an equilibrium-like response to the diurnal temperature cycle, suggesting some reversible absorptive partitioning, but the full dynamic range cannot be reproduced by thermodynamic repartitioning alone. Nighttime aerosol organic nitrate is observed to be positively correlated with $[NO_2] \times [O_3]$ but not with $[O_3]$. These observations support the role of nighttime NO_3-initiated oxidation of monoterpenes as a significant source of nighttime aerosol. Nighttime production of organic nitrates exceeds daytime photochemical production at this site, which we postulate to be representative of the Colorado front range forests.

1 Introduction

Nitrogen oxides affect both daytime and nighttime VOC oxidation mechanisms, in the process controlling tropospheric ozone formation and the branching ratios for production of oxidized VOCs, such as organic peroxides (ROOR and ROOH), alcohols and ketones (ROH and R=O), and multifunctional organic nitrates (RONO2). These products can have reduced volatility making them good aerosol precursors. Figure 1 shows the general mechanisms of NO_x control of VOC oxidation. First, NO_x enhances nighttime or low-light oxidation by providing a source ($NO_2 + O_3$) of elevated NO_3 (blue), adding an additional oxidation pathway. Second, during the day, directly emitted and photolytically produced NO can be elevated (red) and can control the fate of RO_2 radicals, preferentially enhancing RO and $RONO_2$ reaction channel over non-nitrate channels. With sufficiently high NO_3, another nighttime NO_x effect is possible: NO_3 may react with RO_2, effectively playing the role of daytime NO, in competition with $RO_2 + RO_2$ reactions. These reactions remain very poorly understood (Sommariva et al., 2012).

NO_3 is the least understood of the atmospheric oxidants; its concentration is much more variable in space and time and is therefore poorly characterized. Further, since it exists at night in a stable rather than well-mixed boundary layer, surface measurements are insufficient to predict the vertical distribution of NO_3.

Due to its high reactivity, the atmospheric lifetime of NO_3 in forests is likely to be limited by its reaction with unsaturated hydrocarbons, especially biogenic VOCs (Winer et al., 1984; Golz et al., 2001; Fuentes et al., 2007). In urban forests, NO_3 is responsible for a substantial fraction of total VOC degradation (e.g. 28 % in Pabstthum near Berlin, Germany, Geyer et al., 2001).

A better understanding of the effects of NO_x on secondary organic aerosol (SOA) production is a key goal of this study. A growing consensus is emerging that NO_3 initiated oxidation of BVOC is an important source of secondary organic aerosol (Fry et al., 2009, 2011; Pye et al., 2010; Rollins et al., 2012), suggesting that organic nitrates may be a significant fraction of aerosol composition. These nitrates may also contribute to the remaining underprediction of SOA sources: models based on laboratory-measured SOA yields from known precursor VOCs underestimate aerosol loading by from a factor of 2 (Farina et al., 2010) to up to an order of magnitude in polluted regions (de Gouw et al., 2005; Heald et al., 2005; Volkamer et al., 2006) and cannot explain the evolution of SOA (Jimenez et al., 2009). Recent explicit chemical modeling of SOA formation in Mexico City indicate SOA loading increases up to several days downwind of urban areas (Lee-Taylor et al., 2011). All of this suggests the existence of additional mechanisms of SOA formation not yet quantified in the laboratory, yields that are higher under ambient conditions than as measured in the laboratory, or the presence of significant additional VOC mass that is the precursor for aerosol formation (Donahue et al., 2006;

Robinson et al., 2007). More recent modeling results can close the gap with the measurements in polluted regions, but it is unclear if this is for the right reasons (Dzepina et al., 2009; Hodzic et al., 2010). A substantial *enhancement* of biogenic SOA formation due to anthropogenic pollution has been suggested as a controlling factor for SOA formation (de Gouw et al., 2005; Weber et al., 2007; Spracklen et al., 2011; Hoyle et al., 2011). Because NO_x can either suppress or enhance aerosol formation, field measurements that probe NO_x/SOA interactions in the real atmosphere are key to evaluating the magnitude of this effect.

Here, we address the question of the fate of NO_x in a pine forest, with particular focus on its influence on biogenic SOA formation. We measured NO_y (NO_2, peroxynitrates (ΣPNs), alkyl nitrates (ΣANs), and their gas/aerosol partitioning) over a 6-week summertime campaign in a Colorado front range forest, and interpret their daily cycles with the aid of auxiliary data on NO_3, N_2O_5, meteorology, O_3, BVOCs, radicals, and regional transport modeling. We demonstrate and quantify distinct daytime and nighttime mechanisms of organic nitrate formation, showing that even at this forested site 40 km from the nearest urban area (peak $[NO_2] \approx 2$ ppb), NO_x chemistry has a substantial impact on BVOC fate and SOA formation.

2 Experimental design

2.1 BEACHON-RoMBAS field site description

The Bio-hydro-atmosphere interactions of Energy, Aerosols, Carbon, H_2O, Organics, and Nitrogen (BEACHON) project is a long-term, multi-institution, collaborative effort, spearheaded by the National Center for Atmospheric Research (NCAR). In July and August 2011, the Rocky Mountain Biogenic Aerosol Study (BEACHON-RoMBAS, hereinafter RoMBAS) field campaign took place, with research groups from 25 institutions participating in measurements with focus particularly on aerosol emissions and formation. The RoMBAS campaign was located in the United States Forest

Service (USFS) Manitou Forest Observatory (MFO) in Pike National Forest, Colorado (39.10° N, 105.10° W). The site is at 2370 m elevation, 40 km northwest of Colorado Springs and 70 km southwest of Denver, CO (Fig. 2). Vegetation at the site is almost entirely open-canopy ponderosa pine, but nearby areas include Douglas fir, aspen, oak, spruce, willow, and grass which may have some impact at the site. Previous studies at the site have observed dominant VOC emissions to be monoterpenes (34 % of total VOC mixing ratio) and 2-methyl-3-butene-2-ol (MBO, 50 %) during the day, with monoterpene concentrations dominant at night ($\approx 66\%$ of VOC), comprised of a roughly equal mix of α-pinene, β-pinene, and Δ-3-carene (Kim et al., 2010). Night-time winds at the surface were dominated by local drainage flows from the south.

During July and August 2011 the circulation and precipitation patterns over the MFO site were strongly influenced by the North American Monsoon (Hodzic et al., 2012a). During 25–28 July and 2–5 August, the presence of a strong anticyclone over the four-corners region in the southwestern US was associated with the strong southerly mid-level flow, and brought significant amount of moisture from the southeast and southwest into this region. The largest rain event occurred on the evening of 4 August and was characterized by heavy hail and rain whose 5-min intensity values exceed 120 $\mathrm{mm\,h^{-1}}$. During the rest of the campaign, the site was experiencing more zonal synoptic flow with mid-level winds mainly from the west and very little large-scale advection of moisture into the region.

The near surface circulation was strongly influenced by the daytime thermally-induced mountain flow that was established a few hours after sunrise on days when the synoptic forcing was weak. The upslope transport of the Front Range (plains) air and pollution was observed on all nights in NO_2 and some days in CO and SO_2 trace gas measurements (see discussion in Sect. 3.1.2 and Fig. 4).

The site was specifically chosen to have large biogenic emissions and limited anthropogenic influence, and one of the objectives of RoMBAS was studying the ambient submicron aerosol, presumed to be dominantly biogenic. Most chemical instruments

Title Page
Abstract | Introduction
Conclusions | References
Tables | Figures
◀▮ | ▮▶
◀ | ▶
Back | Close
Full Screen / Esc

Printer-friendly Version
Interactive Discussion

were arranged in and on top of trailers with inlets oriented into the dominant wind, towards the south, or on a 30 m tower at the center of the site ("Chemistry tower").

2.2 Instrumentation

Nitrogen dioxide, the sum of total peroxy nitrates (ΣPNs), and the sum of total alkyl nitrates (ΣANs), as well as aerosol-phase only organic nitrates, were measured by a 3-channel thermal dissociation laser induced fluorescence (TD-LIF) instrument similar to that described in Day et al. (2002), with selective measurement of aerosol phase enabled by a modification described in Rollins et al. (2010). Briefly, the instrument thermally dissociates the different classes of NO_y into NO_2 at ambient pressure in three inlet channels, samples this flow through a critical orifice (dropping the pressure to ≈ 2 Torr) into a 38-pass White cell, and measures the NO_2 mixing ratio by LIF at 408 nm. One of these channels can be optionally operated as an "aerosol-only" channel by passing sampled air first through a 10 cm long, 2.2 cm outer diameter cylindrical charcoal denuder (Mast Carbon Ltd, UK NovaCarb F honeycomb monolith, 44 % of cross sectional area open). This denuder removes gases more efficiently than the original design; using calculations described and verified in Rollins et al. (2010), we find that at 10 liters per minute total flow, < 0.001 % of NO_2 gets through this honeycomb charcoal denuder. Contributions of each class of NO_y are determined by calculating the difference in NO_2 concentration detected between the channels. Because peroxynitrates dissociate between 100–150 °C and alkyl nitrates between 250–300 °C, these classes of NO_y can be separately measured, e.g., the difference in NO_2 signal between ambient air sampled through a 180 °C oven (ΣPNs + NO_2) and ambient temperature (NO_2) is attributed to ΣPNs alone. The instrument is calibrated every 3 h using an NO_2 gas standard (4.74 ppm ±2 % NO_2 in N_2, NIST characterized, March 2011, Scott-Marrin) diluted with zero air to 5 known concentrations in the 1–25 ppb range, resulting in a measurement uncertainty of 5 % for NO_2. The accuracy of this measurement and effectiveness of the separation has been demonstrated by comparison to summed individually measured speciated peroxynitrates (Wooldridge et al., 2010) and alkyl nitrates (Perring et al., 2009; Beaver et al., 2012).

The TD-LIF NO_y instrument was run in two modes during the campaign: (1) "3-gas mode", in which the inlet ovens were held at ambient temperature, 180 °C, and 320 °C, with the denuder bypassed, to obtain 1-min averaged timeseries of separated NO_2, ΣPNs, and ΣANs; and (2) "gas-aerosol mode", in which both heated channels are held at 320 °C, with air sampled into one of the heated channels passed through the denuder, to obtain 1-min averaged timeseries of total ΣPNs + ΣANs and aerosol-phase only ΣPNs + ΣANs. It is assumed that the aerosol-phase organic nitrates will consist predominantly of alkyl nitrates, due to the short lifetime of PANs. To the best of our knowledge, PANs have not been measured in the aerosol condensed phase, and a recent intercomparison study of aerosol alkyl nitrates (FTIR) with ΣPNs + ΣANs (TD-LIF) finds that aerosol-phase ΣPNs + ΣANs are dominated by alkyl nitrates (Rollins et al., 2012).

NO_3 and N_2O_5 were measured in situ by cavity ringdown spectroscopy (CRDS) using the 662 nm absorption band of NO_3, detecting N_2O_5 via its thermal conversion to NO_3 (Brown et al., 2001, 2003b, 2007; Wagner et al., 2011). The instrument used a diode laser, tunable over a narrow range near the 662 nm absorption of NO_3, to pump two separate optical cavities, each constructed of two high reflectivity mirrors (R = 99.999 % or better). The laser is modulated as a square wave at 500 Hz, and the single exponential ring-down transients following the falling edge of the square wave are co-added and fit at 4 Hz to measure total optical extinction, α, according to Eq. (1):

$$\alpha = [NO_3]\sigma_{NO_3} = \frac{R_L}{c}\left(\frac{1}{\tau} - \frac{1}{\tau_0}\right) \tag{1}$$

Here τ and τ_0 are exponential intensity decay time constants in the presence and absence of the absorber, respectively, c is the speed of light, R_L is a geometric design factor to account for the fraction of the cavity length occupied by purge volumes that keep the mirrors clean (typically R_L = 1.15), and $[NO_3]$ and $\sigma(NO_3)$ are the NO_3 number density (molecules $\mathrm{cm^{-3}}$) and absorption cross section ($\mathrm{cm^2\,molecule^{-1}}$), respectively. Values of τ_0 vary from 250 to 450 µs, equivalent to 75–135 km in effective path length, to provide sensitivity of 1 pptv (2σ) for NO_3 and N_2O_5. The τ_0 is measured by addition of NO to chemically destroy NO_3 via the rapid reaction $NO + NO_3 \rightarrow 2NO_2$. The combination of 662 nm extinction and NO titration is a specific technique for ambient air NO_3 measurement. The concentration of the sum of NO_3 and N_2O_5 is measured simultaneously by thermal decomposition of N_2O_5 to NO_3 in a second optical cavity that samples through a heated section of tubing (120 °C) and that is maintained at 75 °C. To achieve high sensitivity, both channels sample through a Teflon membrane filter that removes aerosol; filters are changed hourly using an automated device to maintain their cleanliness and transmission of NO_3 and N_2O_5. The instrument has an overall accuracy of ±12 % for the two compounds, calibrated by separately measuring the NO_2 produced from the same chemical titration reaction used to zero the instrument (Fuchs et al., 2008).

Ambient NO_2 was also measured continuously by a chemiluminescent NO_x box (Thermo 17i), which agreed within 8 % with the TD-LIF ambient channel throughout July and August. Inlets for this instrument as well as CO and SO_2 monitors were located at ≈ 3 m. Ozone was measured by UV absorption spectroscopy (2B Technologies, Model 205) and sulfur dioxide by pulsed fluorescence (Thermo Environmental Model 43C-TLE) at 6 different heights along the Chemistry tower (z = 1.6, 5.0, 8.5, 12.0, 17.7 and 25.1 m). These inlets were sampled sequentially every 5 min yielding a complete profile every 30 min; for this work, only concentration data at the lowest height of 1.6 m were used. Carbon monoxide was measured at 3.5 m by a Thermo Environmental Gas Filter Correlation CO analyzer (Model 48 equipped with a heated Pt catalytic converter). Wind speed/direction, temperature and relative humidity were measured at 4 heights (z = 1.8, 7.0, 14.1 and 27.8 m; Vaisala, Model WXT520). Net radiation (visible + IR, incoming – outgoing) was measured at 27.8 m (Radiation and Energy Balance Systems, Inc., Model Q*7.0 net radiometer). Turbulence measurements were made at z = 25.1 m, ≈ 9 m above the canopy height, by a 3-dimensional sonic anemometer (Campbell Scientific, CSAT-3). From these flux measurements, the Obukhov length (L) can be determined (Stull, 1998) which is a surface layer scaling parameter that gives the ratio of buoyant to mechanically (shear) generated turbulence, which can be used a measure of atmospheric stability. When $L > \pm 130$ m ($|z/L| < 0.1$), shear forces dominate and the atmosphere has nearly neutral thermal stability. At values less than ±100 m, convective forces become increasingly important and denote an atmosphere that is either thermally stable ($|z/L| > 0$) or unstable ($|z/L| < 0$).

Volatile organic compounds (VOCs) were measured using two Proton-Transfer-Reaction Time-of-Flight Mass Spectrometers (PTR-ToF-MS, Ionicon Analytik GmbH, Austria (Jordan et al., 2009) and University of Innsbruck (Graus et al., 2010)). Ambient air was sampled at a flow rate of ≈ 9 SLPM through a 40 m long Teflon (PFA) line (1/4″ OD) mounted at 25.3 m on the Chemistry tower. Both instruments were sampling off the same line with a sampling period of about 10 s (NCAR) and 0.1 s (UIBK). The merged dataset was averaged to 6 min. The drift tube was operated at 2.3 mbar (both instruments) and a drift voltage of 580 V (UIBK) and 550 V (NCAR) and a drift tube temperature of 60 °C (both instruments). Calibration was performed by dynamically diluting the VOC standards to ppbv levels using purified ambient air. Details about the data evaluation can be found in Müller et al. (2010), Kaser et al. (2012), and Cappellin et al. (2011).

Submicron particle size distributions (20–800 nm) were measured with a Brechtel Manufacturing, Inc. Scanning Electrical Mobility Spectrometer (SEMS, Model 2002). From these size distributions, total particle surface area per volume can be calculated, and assuming a density of 1.3 g cm^{-3}, aerosol mass loading can be determined.

An Aerodyne high-resolution time-of-flight aerosol mass spectrometer (HR-ToF-AMS; hereafter AMS; DeCarlo et al., 2006), was operated in close vicinity (≈ 10 m NW) to the TD-LIF instrument during RoMBAS. Ambient aerosols in the AMS are analyzed by impaction/vaporization of the aerosol on a porous tungsten vaporizer at 600 °C and subsequent ionization of the gas plume by electron impact; ions are mass analyzed by a high-resolution time-of-flight mass spectrometer. The AMS quantifies non-refractory submicron aerosol, which includes organic species and most inorganic salts and organic species, but not black carbon. Refractory nitrates such as $Ca(NO_3)_2$ and $NaNO_3$ can be detected by the AMS; however, they are typically associated with reacted mineral dust and marine aerosol, respectively, both of which only have small fractions in the submicron regime that were likely negligible during RoMBAS.

The AMS sampled ambient aerosol from an inlet at the same height inside the forest canopy as the TD-LIF instrument; a $PM_{2.5}$ cyclone was used to prevent large dust particles from entering the instrument and sample air was drawn from the inlet into the temperature-controlled trailer through a 3/8 inch o.d. copper tube at 10 lpm. Ambient data used in this work was acquired every 10 min for 2.5-min long intervals using the lower mass-spectral resolution, higher sensitivity mode of the AMS ("V-mode"). The AMS was calibrated every four days with ammonium nitrate aerosol of known mass and calculated submicron aerosol volumes derived from these calibrations agreed well with volumes from a collocated SMPS. The overall accuracy of the AMS for ground measurements has been estimated to be about 30 % (Middlebrook et al., 2012; Hayes et al., 2012), the precision is significantly better: about 4 $ng\,m^{-3}$ for aerosol nitrate and 30 $ng\,m^{-3}$ for OA for the time resolution used here. The low nitrate and high organic aerosol concentrations require careful analysis of the HR spectra, taking into account the contributions of otherwise unimportant isotopic air interferences such as $C^{18}O^+$ and $C^{18}OO^+$ to the signals at *m/z* 30 and 46, respectively.

2.3 Regional modeling

The 3-D Weather Research and Forecasting model coupled with chemistry (WRF-Chem), Grell et al. (2005) was applied to study the transport and chemistry of biogenic and anthropogenic pollutants at the MFO site from 25 July to 26 August 2011. The chemistry was simulated using the SAPRC99 gas-phase chemical mechanism (Carter, 2000) and the MOSAIC aerosol module with 4 size bins (Zaveri et al., 2008). Organic aerosols were treated as described in Hodzic et al. (2012b), and several anthropogenic CO tracers were added to monitor the transport of anthropogenic pollution to the site.

The simulations were performed using two nested domains: a coarse-scale 36-km horizontal resolution grid covering Western and Central US and a fine-scale 4-km grid covering Colorado. The anthropogenic emissions come from the 2005 US EPA National Emission Inventory (NEI), while the biogenic emissions are calculated online using the MEGAN model (Guenther et al., 2006). The initial and boundary conditions for the meteorological variables are taken every 6 h from the NCEP North American Regional Reanalysis, and gas-phase and aerosol variables were obtained from the MOZART4 global chemistry-transport model. The model performance in simulating the meteorology, boundary layer height, and the concentrations of the main gas-phase pollutants during RoMBAS has been evaluated in detail in Hodzic et al. (2012a).

2.4 Predicting gas/aerosol partitioning of organic nitrates

Direct measurements of gas/aerosol partitioning of these organic nitrates can provide insights into relative volatilities of daytime vs. nighttime $RONO_2$, and hence the role of NO_x in SOA formation. Interpreting these observations in terms of chemical mechanisms, however, requires some way to connect chemical structures to a predicted partitioning. We choose to model gas/aerosol partitioning in terms of an absorptive partitioning formalism, following Pankow and Capouet (Pankow, 1994; Capouet and Mul̈ler, 2006). The partitioning coefficient, K_p, is defined as:

$$K_\mathrm{p} = \frac{F/\mathrm{TSP}}{A} = \frac{760 \cdot R \cdot T \cdot f_\mathrm{om}}{\mathrm{MW}_\mathrm{om} \cdot 10^6 \cdot \zeta \cdot p_\mathrm{vap}} \qquad (2)$$

F and A are the total aerosol-phase and gaseous concentrations of the compound of interest, and TSP is the concentration of total suspended particulate matter. In the second expression showing the equilibrium constant in terms of thermodynamic properties, R is the universal gas constant ($8.314\,\mathrm{J\,mol^{-1}\,K^{-1}} = 8.206 \times 10^{-5}\,\mathrm{atm\,m^3\,K^{-1}\,mol^{-1}}$), T is temperature (K), f_om is the weight fraction of organic matter in the total aerosol (assumed = 1), MW_om is the average molecular weight of the absorbing organic material (g mol^{-1}), ζ is the activity coefficient of the compound of interest in the condensed phase (assumed = 1), and p_{vap} is the subcooled vapor pressure of the compound of interest (Torr); 760 (Torr atm^{-1}) and 10^6 (µg g^{-1}) are conversion factors to give K_p in units of m^3 µg^{-1}.

Vapor pressures calculated in this paper are also reported as saturation mass concentrations (C^*) for ease of comparison with volatility basis set parameterizations (Donahue et al., 2006). These saturation densities can be calculated as:

$$C^* = \frac{1}{K_\text{p}} \tag{3}$$

using the same variables shown above to determine K_p, yielding C^* in units of µg m^{-3}.

As pointed out by Barley and McFiggans (2010), a significant uncertainty in this method can arise from the variation in vapor pressure values predicted by different group contribution estimation methods. We use the SIMPOL.1 method here (Pankow and Asher, 2008), with primary focus on the temperature and TSP dependence over a daily cycle for a given molecular structure, rendering the exact predicted p_{vap} values less important than relative changes.

3 Results and discussion

3.1 Reasons for elevated NO_x and organic nitrate concentrations at RoMBAS

3.1.1 Observed diurnal cycles in oxidants, BVOCs, meteorology, and photochemical age markers

Figure 3 shows averaged daily cycles in the concentrations of oxidant and terpenoid gases that form the background and reactants for the observed NO_y chemistry, as well as relevant meteorological variables and an indicator of airmass age with respect to anthropogenic pollution. Ozone (measured at $h = 1.6$ m) shows a typical photochemistry and deposition driven daily cycle, peaking at an average concentration of 60 ppb in the late afternoon and decreasing to 30 ppb during the night. NO_2 shows the opposite diurnal pattern, peaking at an average concentration of 2 ppb at night and sinking below 0.5 ppb during the day. The diurnal NO_2 pattern is explored below in Sect. 3.1.2.

BVOC concentrations measured by PTR-ToF-MS are dominated at night by the sum of all monoterpenes (measured as m/z 137.134 ($C_{10}H_{17}^+$) and m/z 81.071 ($C_6H_9^+$), peak diurnal average concentration of about 0.6 ppb) and during the day by the sum of MBO and isoprene (measured as m/z 87.081 ($C_5H_{11}O^+$) and m/z 69.070 ($C_5H_9^+$), peak average concentration of about 1.8 in the early morning, ≈ 1.5 ppb throughout the day). This suggests a very large daytime photo-induced emission of MBO, since this morning peak occurs simultaneously with an increase in convective vertical mixing which effectively dilutes all species. Furthermore, this morning peak (09:00–10:30 a.m. local time) coincides with an observed downward flux of CO_2 above the canopy (not shown), suggesting a maximum in photosynthetic activity. This transition is shown by the Obukhov stability parameter (z/L in Fig. 3) changing from a positive to negative sign. At this point, the temperature structure switches from a stable nighttime inversion to a daytime positive lapse rate with higher temperatures at the surface. Local wind direction is consistently from the south, with greater variability during the day and early evening.

We also use PTR-ToF-MS measurements of two aromatic hydrocarbons, xylene and benzene, to establish the diurnal changes in average photochemical age of the pollution contained in the airmass. Because xylene and benzene are typically co-emitted by burning related sources which are common in urban areas, their ratio can provide information about photochemical airmass age. Xylene is measured at m/z 107.086 ($C_8H_{11}^+$), as a mixture of *ortho*-, *para*-, and *meta*- isomers, ethylbenzene, and a negligible contributions from the pinonaldehyde fragment. Benzene is measured at m/z 79.055 ($C_6H_7^+$). Both were measured with concentrations in the 10–100 ppt range over the course of the campaign. The time rate of change in the ratio of xylene : benzene provides information on the photochemical age of the airmass; since the OH rate constants of these species are different, the xylene : benzene decreases with aging. We note that this ratio provides no information on the age of the biogenic gases or aerosol in the airmass. This analysis is described below in Sect. 3.1.3.

3.1.2 Information from tracers: modeled and measured

Results from the WRF-Chem simulation from the early part of in the campaign are shown in Fig. 4. The anthropogenic Front Range CO tracers suggests the frequent occurrence of the transport of polluted air from both Denver and Colorado Springs to MFO. This transport occurs in the early afternoon within a well-developed boundary layer. Peaks in observed [SO_2] occur most often during the day, and often coincide with peaks in anthropogenic tracers from either Denver or Colorado Springs, indicating the arrival of pollution plumes at the site. The sharper spikes in predicted surface NO_2 concentrations are also coincident with the presence of anthropogenic tracers at MFO; e.g. the NO_2 spike that was measured and predicted on 27 July is coincident with the modeled arrival of a concentrated Denver plume.

The regular, broader nighttime peaks in NO_2 are also predicted by the model (see e.g. 6–8 August), though the accuracy of the concentration prediction varies. Rather than individual concentrated plumes as for SO_2, this NO_2 appears to arise from a more regional background, consistent with the importance of a few point sources (coal-fired power plants) for SO_2 vs. the much larger contribution of area sources (vehicles) for NO_x. Examination of regional topography (Fig. 2) reveals that the Denver plume could be transported up the Platte River canyon during daytime upslope flow that is characteristic of the Rocky Mountain foothills, and dispersed into the valley where the MFO site is located in late afternoon and evening, potentially leading to these higher nighttime concentrations of urban pollutants. Diurnal variation in measured CO concentration (not shown) almost always tracks NO_2, showing the same broad nighttime peaks, consistent with this idea of a dispersed urban source of NO_2 to MFO.

An alternative explanation for the broad nighttime peaks in NO_2 concentration could be natural emissions of nitrogen oxides from local soils, emitted as NO but immediately titrated to NO_2 by O_3. This appears to be contradicted, however, by the correlation of NO_2 with CO, as well as the observed sharp early evening increases in NO_2 concentration, followed by either flat or decreasing concentrations overnight. If the cause were NO emissions into a shallow nocturnal boundary layer, the concentration increase should continue throughout the night, as observed by, e.g. Aneja et al. (1996). In that study in the southeastern US, the authors used a dynamic flux chamber to quantify the nitrogen flux from soils, which they found to be $\approx 0.1\,\mathrm{ppb}\ NO_2\,\mathrm{h}^{-1}$. Rates of increase observed at RoMBAS were typically of order $1\,\mathrm{ppb}\ NO_2\,\mathrm{h}^{-1}$, with large variability in timing and rate of increase. The terrain and transport at RoMBAS is complex, with downslope drainage flows advecting past the site at night. This makes it far more likely that observed sharp increases in NO_2 is advected in than produced by a soil NO_x source, the buildup of which would if anything be washed out by this drainage flow if it did not contain elevated NO_x.

3.1.3 Observed ambient PANs and ANs

While NO_2 peaks during the night, the diurnal pattern in peroxynitrates (ΣPNs) and alkyl nitrates (ΣANs) is different (top panel of Fig. 5). Both ΣPNs and ΣANs peak during the day, with increases of ≈ 200 ppt in both cases, relative to nighttime concentrations. This increase in concentration occurs coincident with the increased vertical mixing accompanying the switch from nighttime temperature inversion to daytime positive lapse rate, as described in Sect. 3.1.1. A recent comparison (Wooldridge et al., 2010) of ambient ΣPNs measurements shows typical mean concentrations below 500 ppt (except in urban areas where ΣPNs are up to a few ppb), with peak concentration during the day. At another pine forested site downwind of an urban area (BEARPEX, 75 km northeast of Sacramento), mean ΣPNs concentration was ≈ 400 ppt. Also at BEARPEX, ΣANs were found to increase from ≈ 300 ppt to ≈ 600 ppt in the morning (Beaver et al., 2012).

There is no substantial change in local wind direction coincident with the increase in [ΣPNs] and [ΣANs], through the local winds are overall weaker and more mixed in direction during the day than at night. This rules out the possibility that sampling air from a different source region is responsible for the increase. Because the increase in concentration *is* coincident with increasing vertical mixing, a second possible explanation is that higher-NO_y air from above mixes down in the morning. The observations would require that the residual layer above the nocturnal boundary layer consist of essentially NO_2-free air with higher concentrations of ΣPNs and ΣANs, more "aged" forms of NO_y.

The available data does not support a solely vertical mixing explanation for the increase in [ΣPNs] and [ΣANs]; the ratio of xylene to benzene is observed to decrease relatively slowly at daybreak in the mean (Fig. 3). Roberts et al. (1984) showed that fresh emissions have a characteristic ratio of aromatic hydrocarbons, which change with age. In the case of the xylene to benzene ratio, fresh urban emissions have xylene : benzene of 1.3 (Harley et al., 1992) to 2 (Fraser et al., 1998; Schauer et al., 2002). Peak observed xylene : benzene at MFO occurs at night, with an average ratio of ≈ 1. This ratio decreases at daybreak, consistent with photochemical aging, as the rate constant of xylene with OH (1.5×10^{-11} molecules $cm^{-3}\,s^{-1}$, Roberts et al., 1984) is an order of magnitude faster than benzene with OH (1.2×10^{-12} molecules $cm^{-3}\,s^{-1}$, Atkinson et al., 2004). At the observed morning MFO [OH] of 2.5×10^6 molecules cm^{-3} (Kim et al., 2012), these rate constants lead to the prediction that photochemical aging from xylene : benzene of 1 to 0.5 would take ≈ 5–6 h. In fact, we observe this decrease in the ratio over 5 h in the diurnally averaged (mean) data (Fig. 3). Because this change in photochemical age tracks with the increase in [ΣPNs] and [ΣANs] and roughly corresponds to the clock age, we can rule out a large contribution to airmass air from the downward mixing of more aged air aloft in the morning. We note, however, that there are some days on which the xylene : benzene ratio decreases more rapidly, which would be consistent with aged aloft air contributing on occasion.

The final possible explanation for the morning increase in [ΣPNs] and [ΣANs] is that a significant photochemical source exists that initiates at daybreak, converting local VOC that have built up overnight to these more highly oxidized NO_y. This is corroborated by an observed increase in [OH] from 1 to 3×10^6 between 07:00–9:00 a.m. local time (Kim et al., 2012). This photochemical processing is intertwined with tropospheric ozone production, and that chemistry can be used to determine a branching ratio of alkyl nitrate formation in the oxidation of the ambient mixture of VOCs.

3.1.4 Using morning ΣANs rise to determine $RONO_2$ yield and impact on O_3 production

Tropospheric ozone formation is governed by the coupled RO_x and NO_x catalytic cycles. Without radical sinks, typically two O_3 molecules are produced for each time around the RO_x radical cycle ($RO_2 \rightarrow RO \rightarrow HO_2 \rightarrow OH \rightarrow RO_2$), because this drives the $NO \rightarrow NO_2 \rightarrow NO$ cycle twice (Seinfeld and Pandis, 1998, Sect. 5.10). The radical sink (R2) occurs as a minor secondary channel in the $RO_2 + NO$ reaction, the yield of which ($A = R2/(R1 + R2)$) depends on the structure of the initial VOC.

$$RO_2 + NO \rightarrow RO + NO_2 \tag{R1}$$

$$RO_2 + NO \rightarrow RONO_2 \tag{R2}$$

Values of A range from near zero for small hydrocarbons like methane to, e.g. 18 % for α-pinene (Atkinson and Arey, 2003). Because of the coupling of RO_x and NO_x cycles leading to ozone formation, A can be determined empirically by comparing ozone production to alkyl nitrate production when losses (including mixing) of O_3 and $RONO_2$ can be neglected (Rosen et al., 2004):

$$\frac{\Delta O_3}{\Delta \Sigma ANs} \approx \frac{2(1-A)}{A} \approx \frac{2}{A} \tag{4}$$

A is the fractional yield of $RONO_2$ from $RO_2 + NO$ reactions. This analysis would yield a tight, linear correlation if the airmass contained a single reactive hydrocarbon and all radical losses were due to $RO_2 + NO$.

Figure 6 shows ambient O_3 vs. ΣANs for the ≈ 6-day period during which ambient ΣANs were separately measured ("3-gas mode"). In order to omit periods where mixing or deposition of O_3 compete with photochemical production, we include only data from noon to 06:00 p.m. Much of the variability is assumed to be due to the changing ambient mix of VOCs, but additional contributions to the variability may arise from mixing, especially during the morning breakup of the nighttime thermal inversion layer. The fitted slope of 70 ± 18 ($= 2/A$) implies an effective alkyl nitrate yield of $A = 2.9 + 0.3/-0.6\,\%$, similar to a previously observed effective alkyl nitrate yield of 2.4 % in an isoprene-dominated region (Horowitz et al., 2007). The major daytime VOCs at this site are MBO + isoprene (assumed to be dominantly MBO, Kim et al., 2010), with ten times lower concentration of monoterpenes. The OH rate constant with MBO is comparable to that with monoterpenes, but MBO is present at an order of magnitude larger concentration, so RO_2 reactivity is assumed to be dominated by that from MBO. Measured organic nitrate yields from these precursors are available but not well constrained. Alvarado et al. (1999) report a nitrate yield of 5.2 % from MBO; Chan et al. (2009) report 10 ± 4 % yield. The ambient yield of 2.9 % is lower than both MBO lab studies, suggesting either other VOCs contributing to RO_2 chemistry or additional radical losses at the RoMBAS site.

This relatively small ambient alkyl nitrate yield implies that most of the NO_x at the MFO site remains available for ozone production. In the absence of other chain-terminating reactions, the $RONO_2$ yield of 2.9 % would imply a RO_x cycle length of 34; however, other reactions (e.g. $OH + NO_2$, $HO_2 + HO_2$) are likely to contribute and reduce this cycle chain length.

3.2 NO_3 radical fate, nighttime organic nitrate and SOA production

3.2.1 Organic nitrate gas/aerosol partitioning

Examining the NO_y data from "gas/aerosol" mode, we find another interesting diurnal pattern. While total (gas + aerosol-phase) ΣPNs + ΣANs peaks during the day, aerosol-phase only ΣPNs + ΣANs peaks during the night (bottom panel of Fig. 5). This can be seen most clearly in the diurnal cycle of the fraction of ΣPNs + ΣANs in the aerosol phase (black trace, bottom panel of Fig. 5). Up to 30 % of the organic nitrate is in the aerosol phase at night, but less than 10 % during the day. Some of this may be due to repartitioning of semivolatile organic nitrates to the gas phase as temperature increases; however, we show in Sect. 3.2.3 that partitioning thermodynamics alone cannot account for the diurnal pattern observed in the bottom panel of Fig. 5.

3.2.2 Observed and calculated ambient NO_3 and lifetime

Early in the field campaign, the cavity ringdown NO_3/N_2O_5 instrument was deployed to measure in-canopy ambient concentrations for several nights (it was otherwise deployed to monitor oxidant exposure on a NO_3 Potential Aerosol Mass flowtube reactor, manuscript in preparation). On one of those nights, between 23 and 24 July 2011, NO_3 and N_2O_5 displayed a sharp peak just after midnight (shown in the bottom panel of Fig. 7), coincident with a sharp peak in NO_2 and during a period when O_3 was anomalously elevated (55 ppb) until past midnight. In contrast, for most of the remainder of the ambient measurement period, no NO_3 was detectable due high levels of biogenic VOCs that provided a rapid NO_3 sink.

We can use the peak measured $[NO_3] = 5$ ppt, $[NO_2] = 6.5$ ppb, and $[O_3] = 55$ ppb to determine the lifetime of NO_3 due to reactive losses, following the steady-state assumption derived in Eq. (8) of Brown et al. (2003a):

$$\tau_{SS}(NO_3) = \frac{[NO_3]}{k_1[O_3][NO_2]} \approx k_x^{-1} \tag{5}$$

where k_x is the rate constant for reactive loss of NO_3. The lefthand equality of this equation is the definition of the NO_3 steady-state lifetime, and the righthand approximation holds when k_x is the only significant loss term, i.e., when sinks of N_2O_5 are negligible.

In this field campaign, the sinks of N_2O_5 indeed appear to be smaller than reactive loss of NO_3. There are both homogeneous and heterogeneous reactions of N_2O_5 with water, which have been examined extensively (e.g. Brown et al., 2009; Thornton et al., 2003; Wahner et al., 1998; Tuazon et al., 1983; Hjorth et al., 1987). However, the homogeneous $N_2O_5 + H_2O$ rate constant is negligible for this dataset, especially since at 283 K absolute humidity is low (Brown et al., 2007; Crowley et al., 2011). We calculate relative rates of N_2O_5 heterogeneous uptake compared to NO_3 reaction with BVOCs (dominated at night by monoterpenes), using typical nighttime monoterpene (MT), MBO, and sesquiterpene (SQT) concentrations (measured by PTR-ToF-MS) of 0.6 ppb, 0.4 ppb, and 0.01 ppb, respectively, and the N_2O_5/NO_3 ratio of 4.1. This ratio is calculated based on the 283 K equilibrium constant ($K_{eq} = [N_2O_5]/[NO_2][NO_3]$) of $2.05 \times 10^{-10}\,cm^3\,molec^{-1}$ (Sander et al., 2006) and 1 ppb NO_2. The rate constant used for NO_3 with monoterpenes is $6.1 \times 10^{-12}\,cm^3\,molec^{-1}\,s^{-1}$, which is an average of the rate constants with α-pinene, β-pinene, and Δ-3-carene (Calvert et al., 2000), since they were present in roughly equal concentrations at RoMBAS (based on GC/MS canister samples, not shown). For MBO, the 283 K rate constant of $1.1 \times 10^{-14}\,cm^3\,molec^{-1}\,s^{-1}$ is used; for sesquiterpenes, we use the rate constant for β-caryophyllene of $1.9 \times 10^{-11}\,cm^3\,molec^{-1}\,s^{-1}$. At the reported average concentrations, this gives an average NO_3 lifetime ($\tau_{NO_3,BVOC}$) of 14 s, dominated by MT losses (k_i[i] for MT : MBO : SQT is 1 : 0.001 : 0.05).

$$\tau_{NO_3,BVOC} = \frac{1}{k_{NO_3+BVOC}[BVOC]} = \frac{1}{k_{NO_3,MT}[MT] + k_{NO_3,MBO}[MBO] + k_{NO_3,SQT}[SQT]} \quad (6)$$

The heterogeneous uptake of N_2O_5 onto aqueous particles depends on the uptake coefficient (γ), molecular speed of N_2O_5 (v), and the aerosol surface area per volume (SA), parameterized as a first-order rate constant:

$$k_{het} = \frac{\gamma v}{4} SA \quad (7)$$

Measured uptake coefficients on liquid water range from 0.02–0.04 around 283 K (Sander et al., 2006); we use an upper limit value $\gamma = 0.04$. At a typical observed

(SEMS) nighttime aerosol surface area per air volume of 240 $\mu m^2\,cm^{-3}$, N_2O_5 molecular speed of $2.3\times10^4\,cm\,s^{-1}$, this gives an average N_2O_5 lifetime($\tau_{N_2O_5,het}$) of 440 s.

$$\tau_{N_2O_5,het} = \frac{1}{k_{het}} \tag{8}$$

Applying the N_2O_5/NO_3 ratio of 4.1 and comparing to the $\tau_{NO_3,BVOC}$ to $\tau_{N_2O_5,het}$, this estimate suggests that the rate of NO_3 with BVOC is 15 times faster than uptake of N_2O_5 to aqueous particles.

We apply the NO_3 steady-state approximation (Eq. 5) to the case of the high-NO_3 night (23–24 July), to compare the calculated lifetime of NO_3 from steady-state to that calculated from reactive loss via k_x. For the average ambient nighttime temperature of $\approx 283\,K$, $k_1 = 2.3\times10^{-17}\,cm^3\,molec^{-1}\,s^{-1}$ (Atkinson et al., 2004). At the concentrations listed above, this gives $k_x^{-1} = \tau_{SS}(NO_3) = 30\,s$. Calculating the NO_3 lifetime instead from the dominant MT loss ($k_x = k_{NO_3,MT}$), at the observed average MT concentrations that night (7p–5a local) of 0.28 ppb, we find $\tau_{NO_3,MT} = 29\,s$, in excellent agreement with the steady-state prediction. Hence, $N_2O_5 + NO_3$ losses are in fact dominated by reactive loss of NO_3 to biogenic VOCs, with a lifetime in the canopy on the order of seconds, making this a very efficient sink of both species.

Other than the period described above, no NO_3 was observed on four additional nights the CRDS instrument was used to monitor ambient NO_3 and N_2O_5, so it was subsequently deployed to make other measurements. In order to estimate ambient concentrations of NO_3 at RoMBAS throughout the campaign, we can use Eq. (6) to determine an estimate of the NO_3 lifetime, using the known mix, concentration timeseries, and NO_3 rate constants of monoterpenes, sesquiterpenes, and MBO as described above. This calculation shows that maximum NO_3 lifetimes throughout the campaign are consistently < 200 s during the night. The top panel of Fig. 7 shows the result of this calculation, τ_{NO_3}, for the entire campaign. Daytime results have been omitted in this plot, since NO_3 lifetime will be limited by photolysis and reaction with NO during the day.

We also calculate a full timeseries of the production rate of NO_3 based on measured O_3, NO_2, and temperature ($P(NO_3) = k_1[O_3][NO_2]$), shown in the middle panel of Fig. 7. We predict production rates of up to 0.15–0.2 ppt s^{-1} (0.5–0.7 ppb h^{-1}), with peaks generally in the early evening when NO_2 rise and O_3 decline intersect (see Fig. 3). Combining these production and loss terms, we derive the timeseries shown in the bottom panel of Fig. 7, the predicted nighttime steady-state nitrate concentration:

$$NO_{3,SS} = \frac{P(NO_3)}{(\tau_{NO_3,BVOC})^{-1}} \tag{9}$$

Because NO_3 will also be reactively lost to later generation oxidation products, this represents a conservative upper limit on the steady-state concentration of NO_3. During the night of 24 July when peak NO_3 of 5 ppt was measured, our steady-state calculation accurately predicts the timing of the peak, but underestimates its magnitude by almost a factor of 4 (predicted NO_3 concentration was 18 ppt). For most of the campaign, the steady-state NO_3 predicted in this way is significantly lower, near the detection limit of the CRDS instrument, so it may not be surprising that we did not detect it. Golz et al. (2001) also sought to measure NO_3 using DOAS in a European forest and were unable to detect it.

3.2.3 Evidence for NO_3-initiated organic nitrate SOA production at night: (a) predicted organic nitrate structures and modeled thermodynamics

When NO_3 oxidation of monoterpenes is modeled in the Leeds Master Chemical Mechanism (MCMv3.2, http://mcm.leeds.ac.uk/MCM, Jenkin et al. (1997); Saunders et al. (2003)), the major organic nitrates produced by daytime (largely OH-initiated) and nighttime (largely NO_3-initiated) oxidation are distinct (Fig. 8). We carried out two 12-h model runs with the chemical conditions observed at RoMBAS (temperature, $[O_3]$, $[NO_2]$, [monoterpenes]) for daytime photochemistry and dark nighttime chemistry, and tracked the >900 products, identifying the top six organic nitrates in terms of peak concentration during that time period. Daytime simulations were run at 25 °C and 30 % RH, nighttime simulations at 10 °C and 80 % RH. For consistency, both were initiated with the same gas-phase concentrations of reactive precursors: 35 ppb O_3, 4 ppb NO_2, 0.5 ppb α-pinene, 0.4 ppb β-pinene, and 0.1 ppb limonene (Δ-3-carene is not yet in the MCM, and MBO was omitted because it is not expected to produce condensable products).

In both day- and night-time cases, C_{10} hydroxynitrates are among the top products (Fig. 8). The remaining top organic nitrates show some differences, however: during the day, two fragmentation products are observed (outlined in orange), which SIMPOLv.1 predicts to have higher volatility. The structure on the left, a C_9 keto-nitrate, has a predicted vapor pressure of 5.7×10^{-3} Torr at daytime average temperature of 298 K, which is equivalent to a C^* of $6.2 \times 10^4\,\mu g\,m^3$; the structure on the right, a multifunctional peroxynitrate, 1.5×10^{-3} Torr ($C^* = 1.2 \times 10^4\,\mu g\,m^3$). At night, in contrast, two hydroperoxynitrates are observed (outlined in blue), which are predicted to have lower volatility (1.0×10^{-5} Torr at nighttime average temperature of 283 K, $C^* = 130\,\mu g\,m^3$). Hence, accounting for day/night temperature differences observed during RoMBAS, nighttime NO_3-produced organic nitrates have substantially lower volatility, consistent with the observation that a larger fraction of organic nitrates is in the aerosol phase at night.

Although daytime- and nighttime-produced organic nitrates are predicted to be distinct, some of the observed diurnal cycle in aerosol-phase fraction of nitrates (bottom panel of Fig. 5) may be explained by thermodynamics: as temperature cools at night, total organic nitrate repartitions to favor the condensed phase. We can test this null hypothesis by modeling the fraction in the aerosol phase for a series of organic nitrate structures deemed likely as monoterpene oxidation products. We employ the absorptive partitioning formalism introduced in Eq. (2) to predict background aerosol-dependent (using AMS-measured organic aerosol) partitioning of hypothesized structures, using SIMPOLv.1 to predict the temperature-dependent vapor pressures of hypothesized structures. We calculate the average diurnal cycle in several multifunctional nitrates in this way (Fig. 9), using average diurnal cycles in temperature and ambient organic aerosol mass loading as inputs. These model predictions (colors) are shown with comparison to the observed aerosol nitrate fraction (black).

First, we note that neither daytime (C_9 keto-nitrate or PN) nor nighttime (C_{10} hydroperoxy-nitrate) MCM-predicted products would partition appreciably to the aerosol phase in this model: the predicted volatilities are simply too high. As discussed above, Barley and McFiggans (2010) have pointed out that vapor pressure estimation methods differ widely; in a test of sensitivity of calculated OA formation to vapor pressure prediction, Barley and McFiggans observed that predicted multifunctional compounds were 100–1000 times more volatile than needed to contribute significantly to OA.

We find a similar result here. In order to bracket the observed aerosol fraction, one or two additional functional groups must be added (C_{10} keto-hydroxy-nitrate, 2.0×10^{-6} Torr, $C^* = 27\,\mu g\,m^3$ at 283 K; or C_{10} dihydroxy-nitrate, 8.0×10^{-8} Torr, $C^* = 1.0\,\mu g\,m^3$). Alternatively, similarly low volatilities can be realized if the precursor BVOC is a sesquiterpene (C_{15}) with only two functional groups (e.g., C_{10} hydroperoxy-nitrate, 4.6×10^{-8} Torr, $C^* = 0.7\,\mu g\,m^3$ at 283 K). Sesquiterpenes were measured at RoMBAS at much lower concentrations than monoterpenes (nighttime peak < 0.01 ppb, PTR-ToF-MS), but may have a disproportionate impact on aerosol formation because less functionalization is required to achieve lower volatility.

Furthermore, we observe that while the fraction in the aerosol phase falls in the range of these selected tri-functional molecular structures, none of these individual species captures the full dynamic range of aerosol fraction observed. As shown in the bottom panel of Fig. 9, the aerosol fraction is not simply a function of temperature: at the lowest temperatures the observed aerosol fraction is higher than the linear extrapolation that individual structures would predict. This again suggests that at least a subset of the organic nitrates contributing to aerosol during the day and night are in fact of different molecular structures with differing aggregate volatility.

This apparent combination of thermodynamic repartitioning and different production mechanisms of organic nitrates contrasts a recent study (Perraud et al., 2012), in which observed SOA formation from α-pinene could only be explained by irreversible, kinetically-limited uptake of organic nitrates onto aerosol. This difference may be explained by the BVOC precursor mix, if the mechanism is unique to α-pinene, or by the elevated oxidant (1.5 ppm O_3) and aerosol mass (30–2000 $\mu g\,m^3$) in those chamber experiments causing the SOA formation mechanism to be different than under ambient conditions at RoMBAS (30 ppb O_3 and 2 $\mu g\,m^3$ PM_1 at night).

3.2.4 Evidence for NO_3-initiated organic nitrate SOA production at night: (b) oxidant contributions

We find further observational evidence that nighttime chemistry is dominated by NO_3-initiated oxidation rather than ozonolysis when we evaluate their relative rates for all of the campaign nighttime data (Fig. 10). We approximate the rate of $NO_3 + MT$ as the rate of NO_3 production ($P_{NO_3} = k_1[NO_2][O_3]$), because we assume that at night nearly every NO_3 produced is consumed by reaction with monoterpenes. We calculate the ozonolysis rate (R_{O_3+MT}) as $k_O[O_3][MT]$, where $k_O = 5.7 \times 10^{-17}\,cm^3\,molec^{-1}\,s^{-1}$, the average of rates of ozonolysis of α-pinene, β-pinene and Δ-carene (Calvert et al., 2000), the three dominant monoterpenes observed at MFO. We calculate the fraction of monoterpenes oxidized by NO_3 as $P_{NO_3}/(P_{NO_3} + R_{O_3+MT})$ and find that throughout the campaign, 60 % ± 10 % of the nighttime monoterpene reactivity goes via NO_3.

3.3 Aerosol organic nitrate concentrations derived from AMS measurements

The nighttime peak in aerosol organic nitrate concentration is further corroborated by AMS measurements of this species (Fig. 11). Farmer et al. (2010) reported that due to fast thermal dissociation of organic nitrates prior to ionization, the AMS will quantify the nitrate moiety almost exclusively as NO^+ and NO_2^+ ions. Several groups have reported that the NO_2^+/NO^+ ratios observed in AMS spectra for organic nitrates are typically 2–3 times lower than for NH_4NO_3 (Fry et al., 2009; Bruns et al., 2010; Farmer et al., 2010; Liu et al., 2012). Assuming these ratios are stable, the measured ratio can be used to separately quantify ammonium and organic nitrates as (Farmer et al., 2010):

$$\mathrm{RONO}_{2,\mathrm{frac}}=\frac{(R_{\mathrm{ambient}}-R_{\mathrm{NH_4NO_3}})(1+R_{\mathrm{RONO_2}})}{(R_{\mathrm{RONO_2}}-R_{\mathrm{NH_4NO_3}})(1+R_{\mathrm{ambient}})} \tag{10}$$

According to Eq. (10), R_{ambient} (the ratio of NO_2^+/NO^+ in ambient data) can be used to calculate the fraction of organic nitrate, $\mathrm{RONO}_{2,\mathrm{frac}}$, if both $R_{\mathrm{NH_4NO_3}}$ (for the ammonium nitrate calibrant) and $R_{\mathrm{RONO_2}}$ (measured or assumed average NO_2^+/NO^+ for organic nitrates) are known. It should be noted that this expression only applies if NH_4NO_3 is the solely important inorganic nitrate in the submicron mode, since other nitrate salts have different fragmentation ratios. However, as noted above, it is unlikely that reacted dust or seasalt contributed significantly to the submicron aerosol during RoMBAS.

Both $R_{\mathrm{NH_4NO_3}}$ and $R_{\mathrm{RONO_2}}$ depend on the particular AMS instrument and AMS tuning, hence they need to be determined at the same instrument settings as R_{ambient}. While $R_{\mathrm{NH_4NO_3}}$ can be determined from the routine in-field calibrations, estimating $R_{\mathrm{RONO_2}}$ is more difficult as there is some variability in the ratios found for pure organic nitrates (Farmer et al., 2010), and standards for the specific organic nitrates important at a field location are typically not available at the time of the field study. One possible way to circumvent this issue is to use the observation that $R_{\mathrm{NH_4NO_3}}$ and $R_{\mathrm{RONO_2}}$ typically co-vary proportionally between instruments. Based on that observation, we derive field values for $R_{\mathrm{RONO_2}}$ based on previous laboratory measurements of the "ratio of ratios" χ:

$$\chi=\frac{R_{\mathrm{NH_4NO_3}}}{R_{\mathrm{RONO_2}}} \tag{11}$$

Based on the calibrations reported by Farmer et al. (2010), we calculate a value for χ of 2.25 ± 0.35. Using the (very constant) $R_{\mathrm{NH_4NO_3}}$ of 0.295 ± 0.005 measured throughout the in-field IE calibrations, this would result in $R_{\mathrm{RONO_2}} = 0.13 \pm 0.02$.

Figure 11c shows R_{ambient} for ambient data for the six days where the AMS and the TD-LIF ambient aerosol datasets overlap. R_{ambient} is quite constant within the noise at ≈ 0.13, with the exception of a brief spike around midnight of 20 August. This implies that the fraction of total nitrate that is organic was essentially constant, with no diurnal cycle, except for a few brief inorganic nitrate episodes such as on 20 August. Given the very different night and day chemistry, it seems unlikely that this fraction would stay constant, unless it happens to correspond to 100 % organic nitrate, which is consistent with the R_{RONO_2} value derived above.

Another piece of evidence that supports the dominance of organic nitrates in the submicron nitrate at this location is the anion vs. cation balance. A linear regression of measured AMS ammonium vs. predicted, assuming that all measured nitrate is inorganic, leads to a negative intercept and a slope of less than 1 (Fig. 11d; slope = 0.92). The deviation of the slope from 1 is substantially larger than the 2 % observed for NH_4NO_3 calibrations. Such a deviation is normally associated with partially acidic sulfate, but in those cases the deviation typically varies substantially in time (e.g. Zhang et al., 2007), and that would also be expected here given the large variability of SO_2 (Fig. 4). The slope can also be due to mistakenly assuming $RONO_2$ to be inorganic nitrate (Farmer et al., 2010). If we instead exclude all of the aerosol nitrate from the neutralization calculation, the slope becomes very close to 1 (0.99) and the negative intercept disappears. As can be inferred from the tightness of the scatter plot, for most of the campaign this ratio was very constant. While this could reflect an aerosol of fairly constant free acidity, that would be highly unusual for such a long time period. Hence, the most likely explanation is that the anions were fully neutralized and thus most of the nitrate was organic.

Calculated AMS organic nitrate concentrations are compared with the TD-LIF data in Fig. 11a. The overall agreement between the two organic nitrate measurements, both in amplitude and time dependence, is very good, while the TD-LIF dataset appears to have a periodic oscillation. Figure 11b compares AMS organic and inorganic nitrates with the TD-LIF aerosol nitrate. As expected, there is little correlation of TD-LIF nitrate with AMS inorganic nitrate ($r^2 = 0.1$), while the correlation with AMS organic nitrate correlation is fair ($r^2 = 0.53$). Both datasets were averaged to a longer timebase (i.e. longer than the 10 min original database). Given the separate inlets, the low concentrations involved, and the difference in analytical methods, this is a markedly good agreement. The slope for the resampled data, 1.16, seems to indicate a slightly lower AMS response, but is well within the stated accuracies for the instruments (30 % for the AMS, 25 % for the TD-LIF). The dominance of aerosol organic nitrate over the inorganic form at this location contrasts with polluted urban locations such as Riverside, CA, where the aerosol nitrate is dominated by the inorganic form (Farmer et al., 2010).

The concentrations of aerosol organic nitrate concentrations shown in Fig. 11a for both instruments only quantify the NO_3 functional group and do not reflect the actual mass of organic molecules containing nitrate functional groups that are present in the aerosol (since both techniques detect the nitrate functional group after it has dissociated from the organic parent structure). Estimating a total mass for the organic molecules containing nitrate groups is difficult, since the average molecular mass of the organic species per NO_3 group is needed for this calculation. Assuming that the C_{10}-keto-hydroxy-nitrate as shown in Fig. 9 is a representative organic nitrate molecule, the molecular weight of the molecule minus the nitrate group is 168 $\mathrm{g\,mol^{-1}}$, 2.7 times larger than the mass of the nitrate group. For the periods considered here, that implies a concentration of ≈ 0.2–$0.5\,\mathrm{\mu g\,m^{-3}}$ of organic species with nitrate groups, representing 6–20 % of the total organic aerosol mass at a given time. As first reported by Farmer et al. (2010), this also has implications for the O/C and N/C ratios that the AMS reports, since the default analysis algorithm used for field studies assumes that only CHO, CHN, and CHON ions are organic and all of the NO_x^+ ions are assigned to the "nitrate" species. For RoMBAS, including nitrate from $RONO_2$ in the calculation of organic N/C would increase by 0.013 on average (up to 0.025 at night and about 0.009 during the day), while typical AMS N/C values which do not include organic nitrate are ≈ 0.01–0.02 (e.g. Hayes et al., 2012; Docherty et al., 2011). Likewise, O/C ratios would be enhanced 0.03 on average, with spikes of up to 0.07 at night, resulting in about a 5 % increase for the campaign average.

3.4 Estimated alkyl nitrate production rate, daytime vs. nighttime

Finally, we wish to put the nighttime production of alkyl nitrates into context with the total nitrate production. We use our empirically determined daytime yield of $RONO_2$ from $RO_2 + NO$ reactions of 2.9 % (Sect. 3.1.4) to estimate daytime production rates of organic nitrates from OH-initiated reactions followed by $RO_2 + NO$, for comparison to nighttime NO_3-initiated chemistry.

We calculate the daytime production rate of alkyl nitrates as:

$$P_{\text{day}} = (k_{\text{OH}_1}[\text{OH}][\text{MT}] + k_{\text{OH}_2}[\text{OH}][\text{MBO}])A\,F_N \tag{12}$$

where $k_{\text{OH}_1} = 6.5 \times 10^{-11}\,\text{cm}^3\,\text{molec}^{-1}\,\text{s}^{-1}$ (293 K, Rudich et al., 1995) is the rate constant of OH with MBO, and $k_{\text{OH}_2} = 8 \times 10^{-11}\,\text{cm}^3\,\text{molec}^{-1}\,\text{s}^{-1}$ (Calvert et al., 2000) is a representative monoterpene rate constant at this temperature (β-pinene). A is the empirically determined branching ratio of alkyl nitrate production from $RO_2 + NO$ reactions, and F_N is the fraction of RO_2 radicals that react with NO rather than other RO_2 or HO_2. The calculation of this fraction is based on diurnal RO_2 and HO_2 data with calculated NO steady-state concentrations:

$$[\text{NO}]_{\text{ss}} = \frac{[\text{NO}_2]j_{\text{NO}_2}}{k_{\text{O}_3+\text{NO}}\,[\text{O}_3] + k_{\text{R/HO}_2+\text{NO}}\,[\text{RO}_2 + \text{HO}_2]} \tag{13}$$

where j_{NO_2} is the photolysis rate of NO_2, $k_{\text{O}_3+\text{NO}} = 1.4 \times 10^{-12}$ $\exp(-1310/T)\,\text{cm}^3\,\text{molec}^{-1}\,\text{s}^{-1}$ and $k_{\text{R/HO}_2+\text{NO}} = 7.9 \times 10^{-12}\,\text{cm}^3\,\text{molec}^{-1}\,\text{s}^{-1}$, which is the average of rate constants of $HO_2 + NO$ and $CH_3O_2 + NO$ (Sander et al., 2006), using instantaneous measured temperature, $[O_3]$, $[RO_2]$, $[NO_2]$ and $[HO_2]$. Typical daytime $[HO_2]$ peaked midday at 100 ppt; $[RO_2]$ was 45–55 ppt throughout the day, and [NO] peaked at 80 ppt at 08:30 a.m. and 14:30 and was > 40 ppt throughout the day. To determine the relative rates of $RO_2 + NO$ reactions, we use rate constants for CH_3O_2 (Atkinson et al., 2004). We use the CH_3O_2 rate constants because those reactions have been well characterized; however, since they are for a smaller RO_2 than the ambient mix, this likely introduces some error.

Nighttime production rate of alkyl nitrates is calculated as:

$$P_{\text{night}} = [NO_3](k_{\text{MT}}[\text{MT}]Y_{\text{MT}} + k_{\text{MBO}}[\text{MBO}]Y_{\text{MBO}}) \tag{14}$$

where k_i and Y_i are NO_3 rate constants and organic nitrate yields, respectively, from monoterpenes and MBO. Again, we use $6.1 \times 10^{-12}\,\text{cm}^3\,\text{molec}^{-1}\,\text{s}^{-1}$ for the NO_3 + monoterpene rate, the average of rate constants with α-pinene, β-pinene, and Δ-3-carene (Calvert et al., 2000). The rate constant for NO_3 with MBO is $1.1 \times 10^{-14}\,\text{cm}^3\,\text{molec}^{-1}\,\text{s}^{-1}$ (Rudich et al., 1996) at 283 K. Yields of organic nitrates from MT and MBO are taken to be 45 % (Fry et al., 2009, measured nitrate yield for β-pinene) and 13 % (Fantechi et al., 1998), respectively.

Rollins et al. (2012) also recently assessed aerosol organic nitrate yield from NO_3-initiated SOA formation, in Bakersfield, California, an urban site in the agricultural San Joaquin Valley with much higher NO_2, O_3, and biogenic VOC concentrations, and particle loading. At that site, BVOC concentrations are so high that $RONO_2$ production is limited by NO_3 production via $NO_2 + O_3$, which proceeds at typical rates of 1–2 ppb h^{-1} (Rollins et al., 2012). Significantly lower organic nitrate production is observed at RoMBAS (0.05 ppb h^{-1}), due to much lower pollutant concentrations, but at both sites the resulting contribution of $RONO_2$ to organic aerosol loading is substantial.

A comparison of daytime (OH-initiated) and nighttime (NO_3-initiated) rates of alkyl nitrate production is shown in Fig. 12, showing a diurnal cycle that indicates the rates are comparable in magnitude, with the nighttime production rate slightly exceeding daytime. (This analysis omits contributions from ozone, which may contribute to alkyl nitrate formation both during the day and night, but which we cannot constrain.) We note that these production rates are both likely underestimates since they consider only first-generation oxidation chemistry initiated by OH or NO_3, and omit other VOC precursors that may contribute to additional organic nitrate production, e.g. sesquiterpenes. We note further that the empirically-derived A, the daytime organic nitrate branching ratio, implicitly includes any fast chemical losses of daytime $RONO_2$, while the nighttime source calculation is the gross formation rate, with any nighttime $RONO_2$ losses unaccounted for. Based on structural differences – daytime organic nitrates are derived from shorter-chain hydrocarbons and are thus likely to have more oxidized functional groups per carbon and hence be more hydroscopic – we anticipate hydrolysis losses to be faster for daytime than nighttime $RONO_2$. Thus, we believe it is more important that these losses are incorporated for the daytime $RONO_2$ production rate, and we expect the error in net nighttime production rate due to omission of chemical losses to be relatively small.

Because this organic nitrate production is occurring in very different volumes during the day (afternoon boundary layer height of 800–1500 m, radiosonde measurements) vs. night (shallow nocturnal boundary layer height of order 50 to 90 m), the mass of organic nitrate produced during the day is likely to be larger if the NO_x or BVOC level aloft during the night is significantly smaller than that at the surface. Nevertheless, the lower-volatility nighttime organic nitrates produced in the shallower boundary layer lead to a peak in observed aerosol organic nitrate at night. This is consistent with the hypothesis that nighttime NO_3-initiated chemistry is a dominant source of aerosol organic nitrate surface concentrations in the Colorado front range.

4 Conclusions

Substantial morning organic nitrate production is observed at a pine forest site with NO_2 mixing ratios in the 0.5–3 ppb range in the Colorado Front Range, attributed to BVOC reactions with oxidants present in the urban outflow of Denver and Colorado Springs. The fraction of this organic nitrate in the aerosol phase is highest during nighttime, suggesting that nighttime NO_3-initiated chemistry produces more condensable organic nitrates, in addition to thermal repartitioning of all organic nitrates. Comparison of TD-LIF and AMS measurements of organic nitrates shows that aerosol nitrate signal at this site is dominated by organic nitrate, and the aerosol organic nitrate concentrations measured by these two distinct instruments agree very well. Despite the distance from urban centers, NO_3-initiated oxidation is observed to be an important reaction at this site, which is assumed to be representative of forested areas within the Colorado front range foothills. NO_3 radical is responsible for the majority of nighttime monoterpene losses, and contributes substantially to organic aerosol loading.

Acknowledgements. JLF gratefully acknowledges sabbatical support from the Cooperative Institute for Research in Environmental Science (CIRES) and the National Center for Atmospheric Research Visiting Scholars Program. The work was supported in part by NOAA's Atmospheric Chemistry and Climate Program. KJZ was supported by a NASA grant, NNX09AE12G. Measurements conducted by the University of Innsbruck were supported by the Austrian Science Fund (FWF):[L518]; LK is a recipient of a DOC-fFORTE-fellowship of the Austrian Academy of Sciences at the Institute of Ion Physics and Applied Physics. AHR was supported by NSF and by the US DOE grant DE-SC0006711. PCJ, DAD, and JLJ were supported by NSF ATM-0919189. We thank the Cohen research group (UC Berkeley) for the generous instrument loan of the TD-LIF and remote support, especially Drew Rollins, Paul Wooldridge, Kyung-Eun Min, and Ellie Browne. We thank Carsten Warneke, Jim Roberts, Martin Graus, Jim Smith, Peter Harley, and the BEACHON-RoMBAS field campaign team for helpful discussions. We thank the BEACHON project at NCAR (sponsored by NSF) for logistics support during the campaign, and Mike Ryan and the US Forest Service for allowing us to use the Manitou Experimental Forest.

References

Alvarado, A., Tuazon, E., Aschmann, S., Arey, J., and Atkinson, R.: Products and mechanisms of the gas-phase reactions of OH radicals and O-3 with 2-methyl-3-buten-2-ol, Atmos. Environ., 33, 2893–2905, 1999. 1997

Aneja, V., Kim, D.-S., Das, M., and Hartsell, B.: Measurements and analysis of reactive nitrogen species in the rural troposphere of southeast United States: Southern Oxidant Study site SONIA, Atmos. Environ., 30, 649–659, 1996. 1994

Atkinson, R. and Arey, J.: Gas-phase tropospheric chemistry of biogenic volatile organic compounds: a review, Atmos. Environ., 37, Suppl. 2, 197–219, doi:10.1016/S1352-2310(03)00391-1, http://www.sciencedirect.com/science/article/pii/S1352231003003911, 2003. 1996

Atkinson, R., Baulch, D. L., Cox, R. A., Crowley, J. N., Hampson, R. F., Hynes, R. G., Jenkin, M. E., Rossi, M. J., and Troe, J.: Evaluated kinetic and photochemical data for atmospheric chemistry: Volume I - gas phase reactions of O_x, HO_x, NO_x and SO_x species, Atmos. Chem. Phys., 4, 1461–1738, doi:10.5194/acp-4-1461-2004, 2004. 1995, 2000, 2009

Barley, M. H. and McFiggans, G.: The critical assessment of vapour pressure estimation methods for use in modelling the formation of atmospheric organic aerosol, Atmos. Chem. Phys., 10, 749–767, doi:10.5194/acp-10-749-2010, 2010. 1991, 2003

Beaver, M. R., Clair, J. M. St., Paulot, F., Spencer, K. M., Crounse, J. D., LaFranchi, B. W., Min, K. E., Pusede, S. E., Wooldridge, P. J., Schade, G. W., Park, C., Cohen, R. C., and Wennberg, P. O.: Importance of biogenic precursors to the budget of organic nitrates: observations of multifunctional organic nitrates by CIMS and TD-LIF during BEARPEX 2009, Atmos. Chem. Phys., 12, 5773–5785, doi:10.5194/acp-12-5773-2012, 2012. 1986, 1994

Brown, S. S., Stark, H., Ciciora, S., and Ravishankara, A. R.: In-situ measurement of atmospheric NO_3 and N_2O_5 via cavity ring-down spectroscopy, Geophys. Res. Lett., 28, 3227–3230, 2001. 1986

Brown, S. S., Stark, H., and Ravishankara, A. R.: Applicability of the steady state approximation to the interpretation of atmospheric observations of NO_3 and N_2O_5, J. Geophys. Res., 108, doi:10.1029/2003JD003407, 2003a. 1998

Brown, S. S., Stark, H., Ryerson, T., William, E., Nicks, D., Trainer, M., Fehsenfeld, F., and Ravishankara, A. R.: Nitrogen oxides in the nocturnal boundary layer: Simultaneous in situ measurements of NO_3, N_2O_5, NO_2, NO, and O_3, J. Geophys. Res., 108, doi:10.1029/2002jd002917, 2003b. 1986

Brown, S. S., Dubé, W. P., Osthoff, H. D., Wolfe, D. E., Angevine, W. M., and Ravishankara, A. R.: High resolution vertical distributions of NO_3 and N_2O_5 through the nocturnal boundary layer, Atmos. Chem. Phys., 7, 139–149, doi:10.5194/acp-7-139-2007, 2007. 1986, 1999

Brown, S. S., Dube, W., Fuchs, H., Ryerson, T., Wollny, A., Brock, C., Bahreini, R., Middlebrook, A., Neuman, J., Atlas, E., Roberts, J., Osthoff, H., Trainer, M., Fehsenfeld, F., and Ravishankara, A. R.: Reactive uptake coefficients for N_2O_5 determined from aircraft measurements during the Second Texas Air Quality Study: comparison to current model parameterizations, J. Geophys. Res., 114, doi:10.1029/2008JD011679, 2009. 1998

Bruns, E., Perraud, V., Zelenyuk, A., Ezell, M., Johnson, S., Yu, Y., Imre, D., Finlayson-Pitts, B., and Alexander, M.: Comparison of FTIR and particle mass spectrometry for the measurement of particulate organic nitrates, Environ. Sci. Technol., 44, 1056–1061, doi:10.1021/es9029864, 2010. 2005

Calvert, J., Atkinson, J., Kerr, J., Madronich, S., Moortgat, G. K., Wallington, T., and Yarwood, G.: Mechanisms of the Atmospheric Oxidation of the Alkenes, Oxford University Press, New York, NY, USA, 83 pp., 2000. 1999, 2004, 2008, 2009

Capouet, M. and Müller, J.-F.: A group contribution method for estimating the vapour pressures of α-pinene oxidation products, Atmos. Chem. Phys., 6, 1455–1467, doi:10.5194/acp-6-1455-2006, 2006. 1990

Cappellin, L., Biasioli, F., Granitto, P. M., Schuhfried, E., Soukoulis, C., Costa, F., Maerk, T. D., and Gasperi, F.: On data analysis in PTR-TOF-MS: From raw spectra to data mining, Sensor. Actuator. B-Chem., 155, 183–190, 2011. 1988

Carter, W.: Documentation of the SAPRC-99 Chemical Mechanism for VOC Reactivity Assessment, Draft report to the California Air Resources Board, Contracts 92329 and 95308, available at: http://www.cert.ucr.edu/~carter/absts.htm, (last access: November 2012), 2000. 1989

Chan, A., Galloway, M., Kwan, A., Chhabra, P., Keutsch, F., Wennberg, P., Flagan, R., and Seinfeld, J.: Photooxidation of 2-methyl-3-buten-2-ol (MBO) as a potential source of secondary organic aerosol, Environ. Sci. Technol., 43, 4647–4652, doi:10.1021/es802560w, 2009. 1997

Crowley, J. N., Thieser, J., Tang, M. J., Schuster, G., Bozem, H., Beygi, Z. H., Fischer, H., Diesch, J.-M., Drewnick, F., Borrmann, S., Song, W., Yassaa, N., Williams, J., Pöhler, D., Platt, U., and Lelieveld, J.: Variable lifetimes and loss mechanisms for NO_3 and N_2O_5 during the DOMINO campaign: contrasts between marine, urban and continental air, Atmos. Chem. Phys., 11, 10853–10870, doi:10.5194/acp-11-10853-2011, 2011. 1999

Day, D. A., Wooldridge, P. J., Dillon, M., Thornton, J. A., and Cohen, R. C.: A thermal dissociation laser-induced fluorescence instrument for in situ detection of NO_2, peroxy nitrates, alkyl nitrates, and HNO_3, J. Geophys. Res., 107, doi:10.1029/2001JD000779, 2002. 1985

de Gouw, J. A., Middlebrook, A. M., Warneke, C., Goldan, P. D., Kuster, W. C., Roberts, J. M., Fehsenfeld, F. C., Worsnop, D. R., Canagaratna, M. R., Pszenny, A. A. P., Keene, W. C., Marchewka, M., Bertman, S. B., and Bates, T. S.: Budget of organic carbon in a polluted atmosphere: results from the New England Air Quality Study in 2002, J. Geophys. Res.-Atmos., 110, 2005. 1982, 1983

DeCarlo, P., Kimmerl, J., Trimborn, A., Northway, M., Jayne, J., Aiken, A., Gonin, M., Fuhrer, K., Horvath, T., Docherty, K., Worsnop, D., and Jimenez, J.: Field-Deployable, High-Resolution, Time-of-Flight Aerosol Mass Spectrometer, Anal. Chem., 78, 8281–8289, 2006. 1988

Docherty, K. S., Aiken, A. C., Huffman, J. A., Ulbrich, I. M., DeCarlo, P. F., Sueper, D., Worsnop, D. R., Snyder, D. C., Peltier, R. E., Weber, R. J., Grover, B. D., Eatough, D. J., Williams, B. J., Goldstein, A. H., Ziemann, P. J., and Jimenez, J. L.: The 2005 Study of Organic Aerosols at Riverside (SOAR-1): instrumental intercomparisons and fine particle composition, Atmos. Chem. Phys., 11, 12387–12420, doi:10.5194/acp-11-12387-2011, 2011. 2007

Donahue, N. M., Robinson, A. L., Stanier, C. O., and Pandis, S. N.: Coupled partitioning, dilution, and chemical aging of semivolatile organics, Environ. Sci. Technol., 40, 2635–2643, doi:10.1021/es052297c, 2006. 1982, 1991

Dzepina, K., Volkamer, R. M., Madronich, S., Tulet, P., Ulbrich, I. M., Zhang, Q., Cappa, C. D., Ziemann, P. J., and Jimenez, J. L.: Evaluation of recently-proposed secondary organic aerosol models for a case study in Mexico City, Atmos. Chem. Phys., 9, 5681–5709, doi:10.5194/acp-9-5681-2009, 2009. 1983

Fantechi, G., Jensen, N., Hjorth, J., and Peeters, J.: Mechanistic studies of the atmospheric oxidation of methyl butenol by OH radicals, ozone, and NO_3 radicals, Atmos. Environ., 32, 3547–3556, 1998. 2009

Farina, S., Adams, P., and Pandis, S.: Modeling global secondary organic aerosol formation and processing with the volatility basis set: Implications for anthropogenic secondary organic aerosol, J. Geophys. Res., 115, doi:10.1029/2009JD013046, 2010. 1982

Farmer, D., Matsunaga, A., Docherty, K., Surratt, J., Seinfeld, J., Ziemann, P., and Jimenez, J.: Response of an aerosol mass spectrometer to organonitrates and organosulfates and implications for atmospheric chemistry, P. Natl. Acad. Sci. USA, 107, 6670–6675, doi:10.1073/pnas.0912340107, 2010. 2004, 2005, 2006, 2007

Fraser, M. P., Cass, G. R., and Simoneit, B. R. T.: Gas-phase and particle-phase organic compounds emitted from motor vehicle traffic in a Los Angeles roadway tunnel, Environ. Sci. Technol., 32, 2051–2060, doi:10.1021/es970916e, 1998. 1995

Fry, J. L., Kiendler-Scharr, A., Rollins, A. W., Wooldridge, P. J., Brown, S. S., Fuchs, H., Dubé, W., Mensah, A., dal Maso, M., Tillmann, R., Dorn, H.-P., Brauers, T., and Cohen, R. C.: Organic nitrate and secondary organic aerosol yield from NO_3 oxidation of β-pinene evaluated using a gas-phase kinetics/aerosol partitioning model, Atmos. Chem. Phys., 9, 1431–1449, doi:10.5194/acp-9-1431-2009, 2009. 1982, 2005, 2009

Fry, J. L., Kiendler-Scharr, A., Rollins, A. W., Brauers, T., Brown, S. S., Dorn, H.-P., Dubé, W. P., Fuchs, H., Mensah, A., Rohrer, F., Tillmann, R., Wahner, A., Wooldridge, P. J., and Cohen, R. C.: SOA from limonene: role of NO_3 in its generation and degradation, Atmos. Chem. Phys., 11, 3879–3894, doi:10.5194/acp-11-3879-2011, 2011. 1982

Fuchs, H., Dube, W., Ciciora, S., and Brown, S.: Determination of inlet transmission and conversion efficiencies for in situ measurements of the nocturnal nitrogen oxides, NO_3, N_2O_5 and NO_2, via pulsed cavity ring-down spectroscopy, Anal. Chem., 80, 6010–6017, 2008. 1987

Fuentes, J. D., Wang, D., Bowling, D. R., Potosnak, M., Monson, R. K., Goliff, W. S., and Stockwell, W. R.: Biogenic hydrocarbon chemistry within and above a mixed deciduous forest, Journal of Atmospheric Chemistry, 56, 165–185, 2007. 1982

Geyer, A., Alicke, B., Konrad, S., Schmitz, T., Stutz, J., and Platt, U.: Chemistry and oxidation capacity of the nitrate radical in the continental boundary layer near Berlin, J. Geophys. Res., 106, 8013–8025, doi:10.1029/2000JD900681, 2001. 1982

Golz, C., Senzig, J., and Platt, U.: NO_3-initiated oxidation of biogenic hydrocarbons, Chemosphere – Global Change Sci., 3, 339–352, doi:10.1016/S1465-9972(01)00015-0, 2001. 1982, 2001

Graus, M., Mueller, M., and Hansel, A.: High Resolution PTR-TOF: Quantification and Formula Confirmation of VOC in Real Time, J. Am. Soc. Mass Spectr., 21, 1037–1044, doi:10.1016/j.jasms.2010.02.006, 2010. 1988

Grell, G., Peckham, S., Schmitz, R., McKeen, S., Frost, G., Skamarock, W., and Eder, B.: Fully coupled online chemistry within the WRF model, Atmos. Environ., 39, 6957–6975, doi:10.1016/j.atmosenv.2005.04.027, 2005. 1989

Guenther, A., Karl, T., Harley, P., Wiedinmyer, C., Palmer, P. I., and Geron, C.: Estimates of global terrestrial isoprene emissions using MEGAN (Model of Emissions of Gases and Aerosols from Nature), Atmos. Chem. Phys., 6, 3181–3210, doi:10.5194/acp-6-3181-2006, 2006. 1990

Harley, R., Hannigan, M., and Cass, G.: Respeciation of organic gas emissions and the detection of excess unburned gasoline in the atmosphere, Envi. Sci. and Technol., 26, 2395–2408, 1992. 1995

Hayes, P., Ortega, A., Cubison, M., Hu, W., Toohey, D., Flynn, J., Lefer, B., Grossberg, N., Alvarez, S., Rappenglück, B., Taylor, J., Allan, J., Holloway, J., Gilman, J., Kuster, W., de Gouw, J., Massoli, P., Zhang, X., Liu, J., Weber, R., Corrigan, A., Russell, L., Zhao, Y., Cliff, S., Isaacman, G., Worton, D., Kreisberg, N., Hering, S., Goldstein, A., Thalman, R., Waxman, E., Volkamer, R., Lin, Y., Surratt, J., Kleindienst, T., Offenberg, J., Froyd, K., Dusanter, S., Griffith, S., Stevens, P., Brioude, J., Angevine, W., and Jimenez, J. L.: Aerosol composition and sources in Los Angeles during the 2010 CalNex Campaign, J. Geophys. Res. – Atmospheres, submitted, 2012. 1989, 2007

Heald, C. L., Jacob, D. J., Park, R. J., Russell, L. M., Huebert, B. J., Seinfeld, J. H., Liao, H., and Weber, R. J.: A large organic aerosol source in the free troposphere missing from current models, Geophys. Res. Lett., 32, doi:10.1029/2005GL023831, 2005. 1982

Hjorth, J., Ottobrini, G., Cappellani, F., and Restelli, G.: A Fourier transform infrared study of the rate constant of the homogeneous gas-phase reaction nitrogen oxide (N_2O_5) + water and determination of absolute infrared band intensities of N_2O_5 and nitric acid, J. Phys. Chem., 91, 1565–1568, doi:10.1021/j100290a055, 1987. 1999

Hodzic, A., Jimenez, J. L., Madronich, S., Canagaratna, M. R., DeCarlo, P. F., Kleinman, L., and Fast, J.: Modeling organic aerosols in a megacity: potential contribution of semi-volatile and intermediate volatility primary organic compounds to secondary organic aerosol formation, Atmos. Chem. Phys., 10, 5491–5514, doi:10.5194/acp-10-5491-2010, 2010. 1983

Hodzic, A., Gochis, D., Chen, F., et al.: Meteorological conditions, emissions and transport of pollutants over the Rocky Mountains region during the 2011 BEACHON-ROMBAS field study, in preparation, 2012a. 1984, 1990

Hodzic, A., Wiedinmyer, C., Salcedo, D., and Jimenez, J.: Impact of trash burning on air quality in Mexico City, Environ. Sci. Technol., 46, 4950–4957, doi:10.1021/es203954r, 2012b. 1989

Horowitz, L. W., Fiore, A. M., Milly, G. P., Cohen, R. C., Perring, A., Wooldridge, P. J., Hess, P. G., Emmons, L. K., and Lamarque, J.-F.: Observational constraints on the chemistry of isoprene nitrates over the eastern United States, J. Geophys. Res., 112, D12S08, doi:10.1029/2006JD007747, 2007. 1997

Hoyle, C. R., Boy, M., Donahue, N. M., Fry, J. L., Glasius, M., Guenther, A., Hallar, A. G., Huff Hartz, K., Petters, M. D., Petäjä, T., Rosenoern, T., and Sullivan, A. P.: A review of the anthropogenic influence on biogenic secondary organic aerosol, Atmos. Chem. Phys., 11, 321–343, doi:10.5194/acp-11-321-2011, 2011. 1983

Jenkin, M., Saunders, S., and Pilling, M.: The tropospheric degradation of volatile organic compounds: a protocol for mechanism development, Atmos. Environ., 31, 81–104, doi:10.1016/S1352-2310(96)00105-7, 1997. 2001

Jimenez, J. L., Canagaratna, M. R., Donahue, N. M., Prevot, A. S. H., Zhang, Q., Kroll, J. H., DeCarlo, P. F., Allan, J. D., Coe, H., Ng, N. L., Aiken, A. C., Docherty, K. S., Ulbrich, I. M., Grieshop, A. P., Robinson, A. L., Duplissy, J., Smith, J. D., Wilson, K. R., Lanz, V. A., Hueglin, C., Sun, Y. L., Tian, J., Laaksonen, A., Raatikainen, T., Rautiainen, J., Vaattovaara, P., Ehn, M., Kulmala, M., Tomlinson, J. M., Collins, D. R., Cubison, M. J., E., Dunlea, J., Huffman, J. A., Onasch, T. B., Alfarra, M. R., Williams, P. I., Bower, K., Kondo, Y., Schneider, J., Drewnick, F., Borrmann, S., Weimer, S., Demerjian, K., Salcedo, D., Cottrell, L., Griffin, R., Takami, A., Miyoshi, T., Hatakeyama, S., Shimono, A., Sun, J. Y., Zhang, Y. M., Dzepina, K., Kimmel, J. R., Sueper, D., Jayne, J. T., Herndon, S. C., Trimborn, A. M., Williams, L. R., Wood, E. C., Middlebrook, A. M., Kolb, C. E., Baltensperger, U., and Worsnop, D. R.: Evolution of organic aerosols in the atmosphere, Science, 1525–1529, doi:10.1126/science.1180353, 2009. 1982

Jordan, A., Haidacher, S., Hanel, G., Hartungen, E., Mark, L., Seehauser, H., Schottkowsky, R., Sulzer, P., and Mark, T.: A high resolution and high sensitivity proton-transfer-reaction time-of-flight mass spectrometer (PTR-TOF-MS), Intl. J. Mass Spectrom., 286, 122–128, doi:10.1016/j.ijms.2009.07.005, 2009. 1988

Kaser, L., Karl, T., Schnitzhofer, R., Graus, M., Herdlinger-Blatt, I. S., DiGangi, J. P., Sive, B., Turnipseed, A., Hornbrook, R. S., Zheng, W., Flocke, F. M., Guenther, A., Keutsch, F. N., Apel, E., and Hansel, A.: Comparison of different real time VOC measurement techniques in a ponderosa pine forest, Atmos. Chem. Phys. Discuss., 12, 27955-27988, doi:10.5194/acpd-12-27955-2012, 2012. 1988

Kim, S., Karl, T., Guenther, A., Tyndall, G., Orlando, J., Harley, P., Rasmussen, R., and Apel, E.: Emissions and ambient distributions of Biogenic Volatile Organic Compounds (BVOC) in a ponderosa pine ecosystem: interpretation of PTR-MS mass spectra, Atmos. Chem. Phys., 10, 1759–1771, doi:10.5194/acp-10-1759-2010, 2010. 1984, 1997

Kim, S., Wolfe, G. M., Mauldin, L., Cantrell, C., Guenther, A., Karl, T., Turnipseed, A., Greenberg, J., Hall, S. R., Ullmann, K., Apel, E., Hornbrook, R., Kajii, Y., Nakashima, Y., Keutsch, F. N., DiGangi, J. P., Henry, S. B., Kaser, L., Schnitzhofer, R., Graus, M., and Hansel, A.: Evaluation of HOx sources and cycling using measurement-constrained model calculations in a 2-methyl-3-butene-2-ol (MBO) and monoterpene (MT) dominated ecosystem, Atmos. Chem. Phys. Discuss., 12, 15945–15975, doi:10.5194/acpd-12-15945-2012, 2012. 1995

Lee-Taylor, J., Madronich, S., Aumont, B., Baker, A., Camredon, M., Hodzic, A., Tyndall, G. S., Apel, E., and Zaveri, R. A.: Explicit modeling of organic chemistry and secondary organic aerosol partitioning for Mexico City and its outflow plume, Atmos. Chem. Phys., 11, 13219–13241, doi:10.5194/acp-11-13219-2011, 2011. 1982

Liu, S., Shilling, J., Song, C., Hiranuma, N., Zaveri, R., and Russell, L.: Hydrolysis of organonitrate functional groups in aerosol particles, Aerosol. Sci. Tech., 46, 1359–1369, doi:10.1080/02786826.2012.716175, 2012. 2005

Middlebrook, A., Bahreini, R., Jimenez, J., and Canagaratna, M.: Evaluation of composition-dependent collection efficiencies for the aerodyne aerosol mass spectrometer using field data, Aerosol. Sci. Tech., 46, 258–271, doi:10.1080/02786826.2011.620041, 2012. 1989

Müller, M., Graus, M., Ruuskanen, T. M., Schnitzhofer, R., Bamberger, I., Kaser, L., Titzmann, T., Hörtnagl, L., Wohlfahrt, G., Karl, T., and Hansel, A.: First eddy covariance flux measurements by PTR-TOF, Atmos. Meas. Tech., 3, 387–395, doi:10.5194/amt-3-387-2010, 2010. 1988

Pankow, J. F.: An absorption-model of gas-particle partitioning of organic-compounds in the atmosphere, Atmos. Environ., 28, 185–188, 1994. 1990

Pankow, J. F. and Asher, W. E.: SIMPOL.1: a simple group contribution method for predicting vapor pressures and enthalpies of vaporization of multifunctional organic compounds, Atmos. Chem. Phys., 8, 2773–2796, doi:10.5194/acp-8-2773-2008, 2008. 1991

Perraud, V., Bruns, E. A., Ezell, M. J., Johnson, S. N., Yu, Y., Alexander, M. L., Zelenyuk, A., Imre, D., Chang, W. L., Dabdub, D., Pankow, J. F., and Finlayson-Pitts, B. J.: Nonequilibrium atmospheric secondary organic aerosol formation and growth, PNAS, doi:10.1073/pnas.1119909109, 2012. 2004

Perring, A. E., Wisthaler, A., Graus, M., Wooldridge, P. J., Lockwood, A. L., Mielke, L. H., Shepson, P. B., Hansel, A., and Cohen, R. C.: A product study of the isoprene + NO_3 reaction, Atmos. Chem. Phys., 9, 4945–4956, doi:10.5194/acp-9-4945-2009, 2009. 1986

Pye, H. O. T., Chan, A. W. H., Barkley, M. P., and Seinfeld, J. H.: Global modeling of organic aerosol: the importance of reactive nitrogen (NO_x and NO_3), Atmos. Chem. Phys., 10, 11261–11276, doi:10.5194/acp-10-11261-2010, 2010. 1982

Roberts, J., Fehsenfeld, F., Liu, S., Bollinger, M., Hahn, C., Albritton, D., and Sievers, R.: Measurements of aromatic hydrocarbon ratios and NO_x concentrations in the rural troposphere – observation of air mass photochemical aging and NO_x removal, Atmos. Environ., 18, 2421–2432, 1984. 1995

Robinson, A. L., Donahue, N. M., Shrivastava, M. K., Weitkamp, E. A., Sage, A. M., Grieshop, A. P., Lane, T. E., Pierce, J. R., and Pandis, S. N.: Rethinking organic aerosols: semivolatile emissions and photochemical aging, Science, 315, 1259–1262, doi:10.1126/science.1133061, http://www.sciencemag.org/content/315/5816/1259.abstract, 2007. 1983

Rollins, A. W., Smith, J., Wilson, K., and Cohen, R. C.: Real time in situ detection of organic nitrates in atmospheric aerosols, Environ. Sci. Technol., 44, 5540–5545, doi:10.1021/es100926x, 2010. 1985

Rollins, A. W., Browne, E. C., Min, K.-E., Pusede, S. E., Wooldridge, P. J., Gentner, D. R., Goldstein, A. H., Liu, S., Day, D. A., Russell, L. M., and Cohen, R. C.: Evidence for NO_x control over nighttime SOA formation, Science, 337, 1210–1212, doi:10.1126/science.1221520, 2012. 1982, 1986, 2009

Rosen, R. S., Wood, E. C., Wooldridge, P. J., Thornton, J. A., Day, D. A., Kuster, W., Williams, E. J., Jobson, B. T., and Cohen, R. C.: Observations of total alkyl nitrates during Texas Air Quality Study 2000: implications for O_3 and alkyl nitrate photochemistry, J. Geophys. Res., 109, D07 303, doi:10.1029/2003JD004227, 2004. 1996

Rudich, Y., Talukdar, R. K., Burkholder, J. B., and Ravishankara, A. R.: The reaction of methyl butenol with OH radical: mechanism and atmospheric implications, J. Phys. Chem., 99, 12 188–12 194, 1995. 2008

Rudich, Y., Talukdar, R. K., Fox, R. W., and Ravishankara, A. R.: Rate coefficients for reactions of NO_3 with a few olefins and oxygenated olefins, J. Phys. Chem., 100, 5374–5381, 1996. 2009

Sander, S. P., Friedl, R. R., Golden, D. M., kurylo, M. J., Moortgat, G. K., Keller-Rudek, H., Wine, P. H., Ravishankara, A. R., Kolb, C. E., Molina, M. J., Finlayson-Pitts, B. J., and Huie, R. E.: Chemical Kinetics and Photochemical Data for Use in Atmospheric Studies, Evaluation Number 15, 2006. 1999, 2008

Saunders, S. M., Jenkin, M. E., Derwent, R. G., and Pilling, M. J.: Protocol for the development of the Master Chemical Mechanism, MCM v3 (Part A): tropospheric degradation of non-aromatic volatile organic compounds, Atmos. Chem. Phys., 3, 161–180, doi:10.5194/acp-3-161-2003, 2003. 2001

Schauer, J. J., Kleeman, M. J., Cass, G. R., and Simoneit, B. R. T.: Measurement of emissions from air pollution sources. 5. C_1-C_{32} organic compounds from gasoline-powered motor vehicles, Environ. Sci. Technol., 36, 1169–1180, doi:10.1021/es0108077, 2002. 1995

Seinfeld, J. H. and Pandis, S. N.: Atmospheric Chemistry and Physics: From Air Pollution to Climate Change, 1998. 1996

Sommariva, R., Bates, T. S., Bon, D., Brookes, D. M., de Gouw, J. A., Gilman, J. B., Herndon, S. C., Kuster, W. C., Lerner, B. M., Monks, P. S., Osthoff, H. D., Parker, A. E., Roberts, J. M., Tucker, S. C., Warneke, C., Williams, E. J., Zahniser, M. S., and Brown, S. S.: Modelled and measured concentrations of peroxy radicals and nitrate radical in the U.S. Gulf Coast region during TexAQS 2006, J. Atmos. Chem., 68, 331–362, doi:10.1007/s10874-012-9224-7, 2011. 1982

Spracklen, D. V., Jimenez, J. L., Carslaw, K. S., Worsnop, D. R., Evans, M. J., Mann, G. W., Zhang, Q., Canagaratna, M. R., Allan, J., Coe, H., McFiggans, G., Rap, A., and Forster, P.: Aerosol mass spectrometer constraint on the global secondary organic aerosol budget, Atmos. Chem. Phys., 11, 12109–12136, doi:10.5194/acp-11-12109-2011, 2011. 1983

Stull, R.: An Introduction to Boundary Layer Meteorology, Springer, 1998. 1988

Thornton, J., Braban, C., and Abbatt, J.: N_2O_5 hydrolysis on sub-micron organic aerosols: the effect of relative humidity, particle phase, and particle size, Phys. Chem. Chem. Phys., 5, 4593–4603, 2003. 1998

Tuazon, E. C., Atkinson, R., Plum, C. N., Winer, A. M., and Pitts, J. N.: The reaction of gas phase N_2O_5 with water vapor, Geophys. Res. Lett., doi:10.1029/GL010i010p00953, 10, 953–956, 1983. 1999

Volkamer, R., Jimenez, J., San Martini, F., Dzepina, K., Zhang., Q., Salcedo, D., Molina, L., Worsnop, D., and Molina, M.: Secondary organic aerosol formation from anthropogenic air pollution: Rapid and higher than expected, Geophys. Res. Lett., 33, doi:10.1029/2006GL026899, 2006. 1982

Wagner, N., Dube, W., Washenfelder, R., Young, C., Pollack, I., Ryerson, T., and Brown, S.: Diode laser-based cavity ring-down instrument for NO_3, N_2O_5, NO, NO_2 and O_3 from aircraft, Atmos. Meas. Tech., 4, 1227–1240, doi:10.5194/amt-4-1227-2011, 2011. 1986

Wahner, A., Mentel, T. F., and Sohn, M.: Gas-phase reaction of N_2O_5 with water vapor: Importance of heterogeneous hydrolysis of N_2O_5 and surface desorption of HNO_3 in a large Teflon chamber, Geophys. Res. Lett., 25, 2169–2172, doi:10.1029/98GL51596, 1998. 1999

Weber, R., Sullivan, A., Peltier, R., Russell, A., Yan, B., Zheng, M., de Gouw, J., Warneke, C., Brock, C., Holloway, J., Atlas, E., and Edgerton, E.: A study of secondary organic aerosol formation in the anthropogenic-influenced southeastern United States, J. Geophys. Res., 112, D13302, doi:10.1029/2007JD008408, 2007. 1983

Winer, A. M., Atkinson, R., and Pitts, J. N.: Gaseous nitrate radical: possible nighttime atmospheric sink for biogenic organic compounds, Science, 224, 156–159, 1984. 1982

Wooldridge, P. J., Perring, A. E., Bertram, T. H., Flocke, F. M., Roberts, J. M., Singh, H. B., Huey, L. G., Thornton, J. A., Wolfe, G. M., Murphy, J. G., Fry, J. L., Rollins, A. W., LaFranchi, B. W., and Cohen, R. C.: Total Peroxy Nitrates (ΣPNs) in the atmosphere: the Thermal Dissociation-Laser Induced Fluorescence (TD-LIF) technique and comparisons to speciated PAN measurements, Atmos. Meas. Tech., 3, 593–607, doi:10.5194/amt-3-593-2010, 2010. 1986, 1994

Zaveri, R. A., Easter, R. C., Fast, J. D., and Peters, L. K.: Model for Simulating Aerosol Interactions and Chemistry (MOSAIC), J. Geophys. Res., 113, doi:10.1029/2007JD008782, 2008. 1989

Zhang, Q., Jimenez, J., Worsnop, D., and Canagaratna, M.: A case study of urban particle acidity and its effect on secondary organic aerosol, Environ. Sci. Technol., 41, 3213–3219, doi:10.1021/es061812j, 2007. 2006

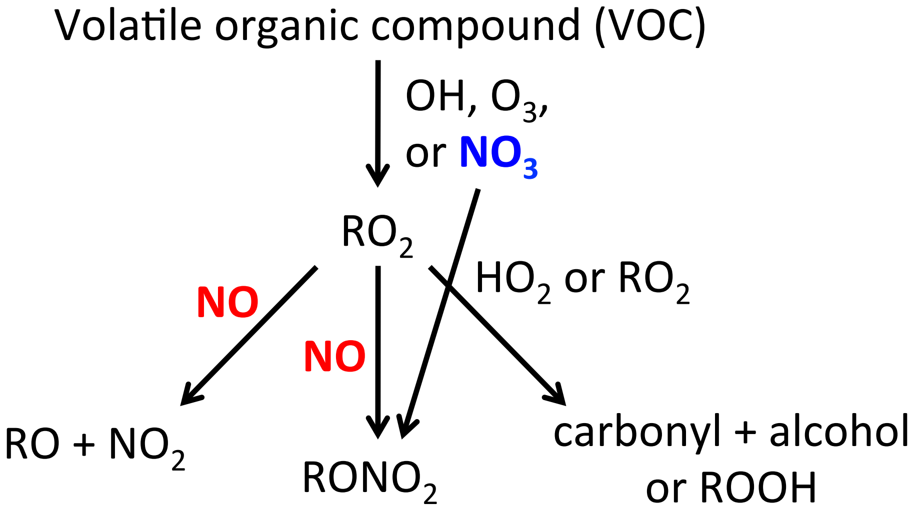

Fig. 1. Overview of potential NO_x effects on the oxidation of a volatile organic compound.

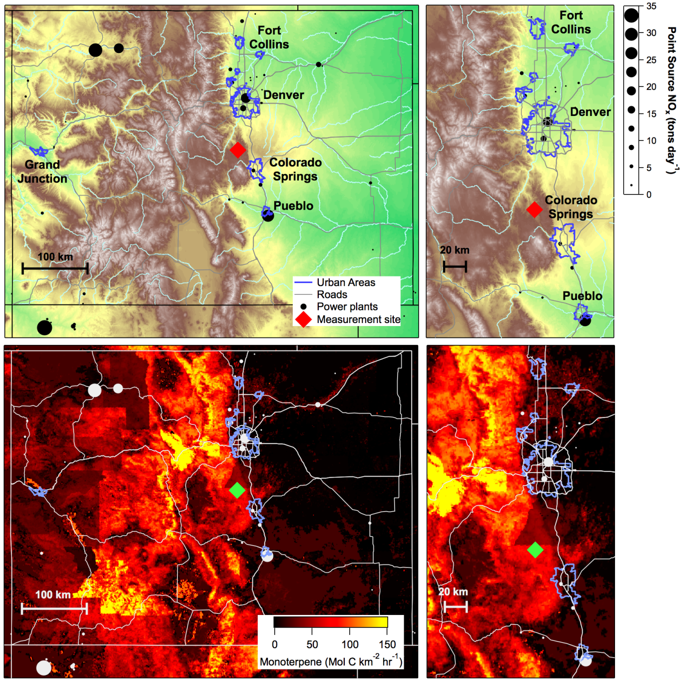

Fig. 2. Map of Manitou Forest Observatory site. Top panels show topography and point sources for NO_x. Regional NO_x point sources are shown as black/grey dots with size proportional to emissions rate. The Four Corners power plant (lower left of larger map) is not shown on this scale; its emissions of 136 tons day^{-1} dwarf all other power plants in this region. The site is 40 km northwest of Colorado Springs and 70 km southwest of Denver, the two largest urban areas (outlined in blue) in the domain. For discussion of transport to the site, note the South Platte River Valley (rivers shown in aqua) southwest from the Denver urban area towards the field site (red/green diamond). Bottom panels show monoterpene emissionf potential, calculated using the BEIS model.

ACPD

13, 1979–2034, 2013

Observations of gas- and aerosol-phase organic nitrates

J. L. Fry et al.

Title Page
Abstract | Introduction
Conclusions | References
Tables | Figures
◀I | ▶I
◀ | ▶
Back | Close
Full Screen / Esc
Printer-friendly Version
Interactive Discussion

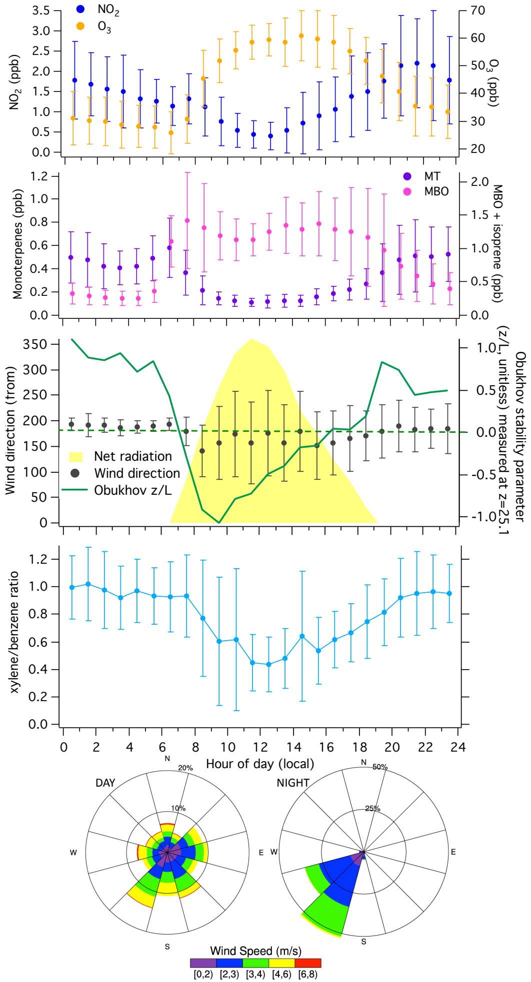

Fig. 3. Please see caption on next page.

Fig. 3. Hourly binned average diurnal trends in NO_2 (blue), O_3 (orange), monoterpenes (purple), methyl butenol and isoprene (pink), wind direction (grey), radiation (yellow, arbitrary units), Obukhov length (green), xylene to benzene ratio (aqua), and average day and night windroses at MFO, 21 July–24 August 2011. Error bars are 1σ based on data averaged to a one-hour timebase; all points are averaged for the same hour intervals but offset slightly on some plots to make error bars easier to read. Concentrations of NO_2 and monoterpenes peak at night when they are concentrated in a shallow boundary layer, while O_3 and MBO peak during the day. Winds are dominantly from the south, with more variability during the day; every morning at sunrise the Obukhov length shows a transition from a stable nighttime inversion to a convectively mixed boundary layer, and decreasing xylene:benzene ratio shows aging.

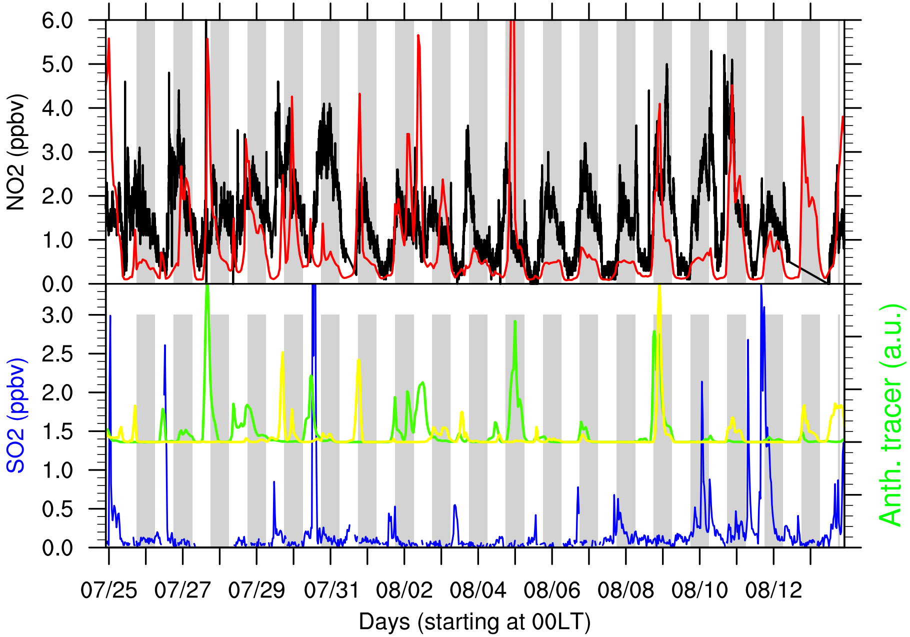

Fig. 4. Time series of NO_2 (black, Thermo 17i) and SO_2 (blue) surface concentrations as observed at the MFO site during the early stages of RoMBAS from 26 July to 14 August 2011. The WRF-Chem predicted NO_2 is also shown (red, ppbv), as well as the levels of advected anthropogenic tracers (arbitrary units) from Denver (green) and Colorado Springs (yellow). Gray shadings indicate nighttime periods (8 p.m.–8 a.m.).

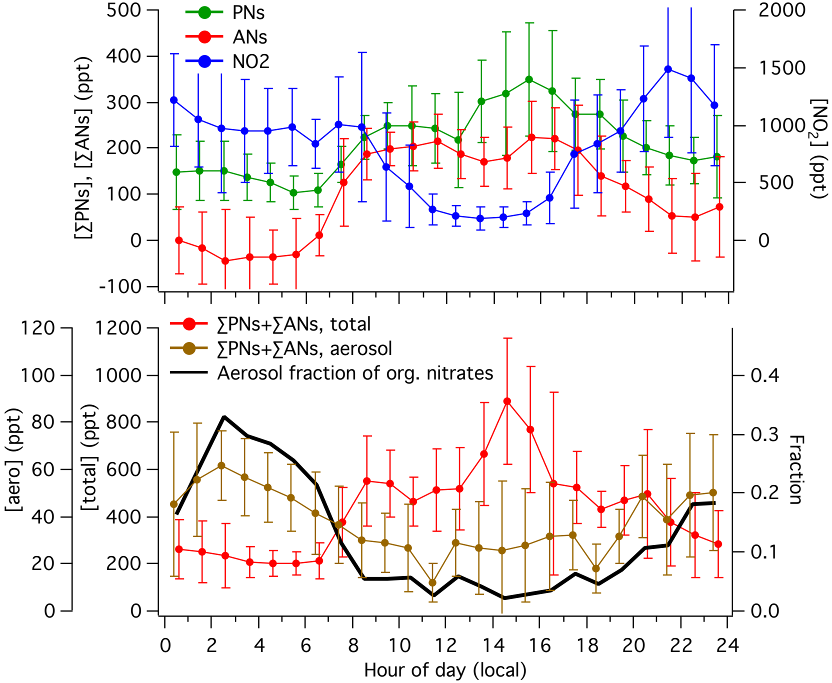

Fig. 5. Hourly binned average diurnal trends in (top): NO$_2$ (blue), ΣPNs (green), and ΣANs (red) from times when the TD-LIF was running in "3-gas" mode (13–17 and 19–20 August); and (bottom): total ΣPNs + ΣANs (red), aerosol-phase only ΣPNs + ΣANs (brown), and fraction of organic nitrates in the aerosol phase (black) from times when the TD-LIF was running in "gas/aerosol" mode (28 July–1 August, 20–22 August). Error bars are 1σ based on data averaged to a one-hour timebase; all points are averaged for the same hour intervals but offset slightly on some plots to make error bars easier to read. The NO$_2$ trace looks slightly different than Fig. 3 because this data comes only from the subset of campaign days when the TD-LIF was running in "gas/aerosol" ambient mode.

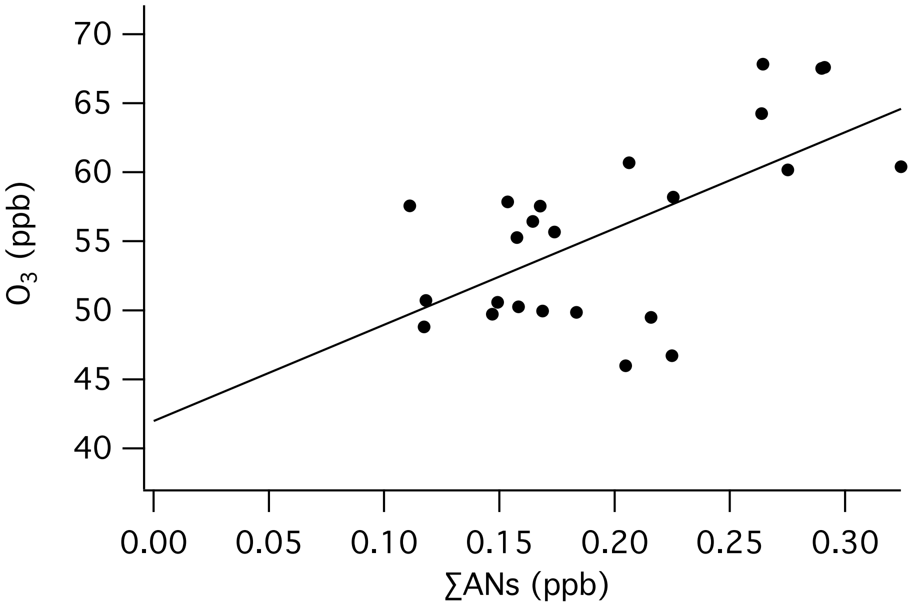

Fig. 6. Correlation plot of measured ambient O_3 vs. ΣANs, for the ≈ 6 days during the campaign when the TD-LIF was running in "3-gas" ambient mode, with standard linear regression, slope = 70 ± 18. Only data from 12 noon – 6 p.m. local time are used.

Title Page
Abstract | Introduction
Conclusions | References
Tables | Figures
◀| |▶
◀ ▶
Back | Close
Full Screen / Esc

Printer-friendly Version

Interactive Discussion

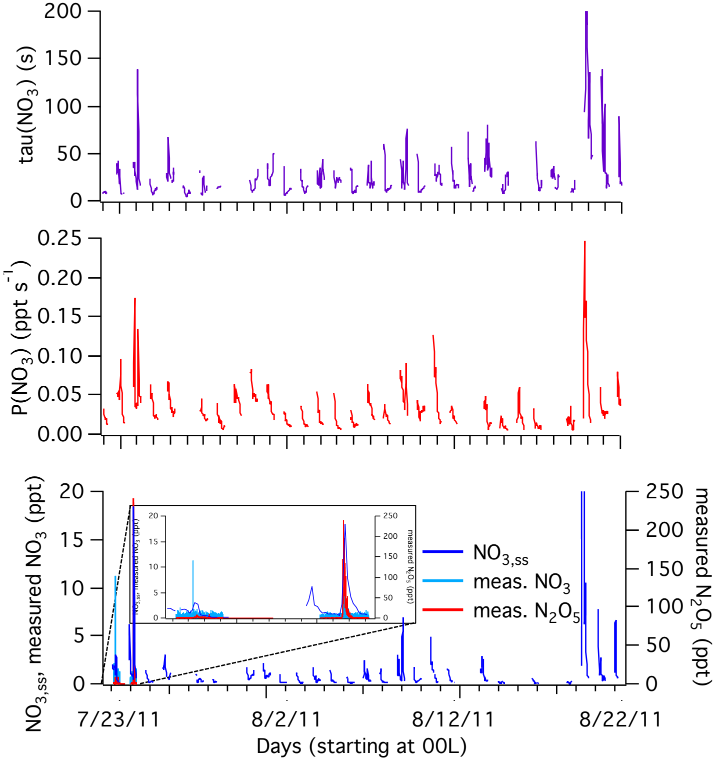

Fig. 7. Calculated lifetime based on BVOC reactive losses (top, purple), production rate from $NO_2 + O_3$ (middle, red) and predicted steady-state concentration (lower, blue) of NO_3 throughout the RoMBAS campaign, nights only. Lower panel also shows measured NO_3 (aqua) and N_2O_5 (red) from two nights early in the campaign.

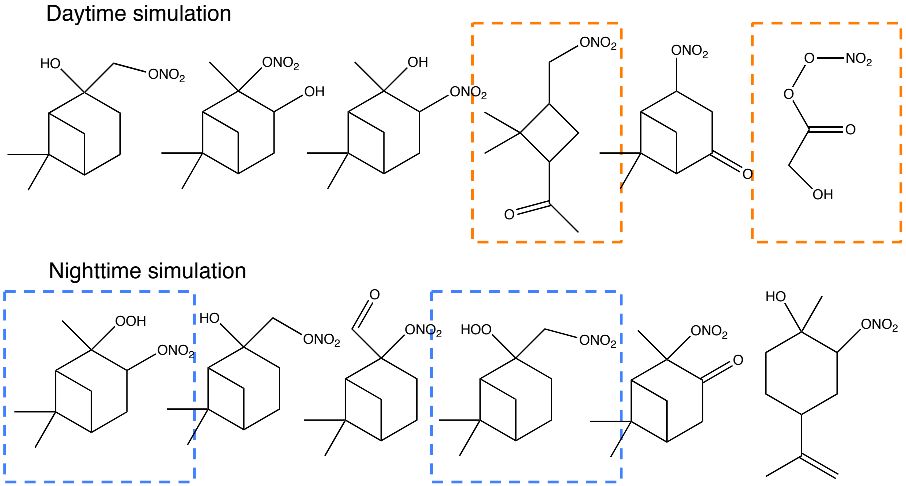

Fig. 8. Major organic nitrate oxidation products predicted by the MCM for daytime and nighttime simulations, initialized with observed monoterpene and oxidant concentrations at MFO. Structures are shown in order of peak concentration, with highest on the left. Outlined structures show the more volatile daytime nitrates (predicted $p_{\mathrm{vap}} > 10^{-3}$ Torr; $C^* > 10^4\,\mu\mathrm{g\,m}^3$) and less volatile nighttime nitrates (predicted $p_{\mathrm{vap}} \approx 10^{-5}$ Torr; $C^* \approx 100\,\mu\mathrm{g\,m}^3$).

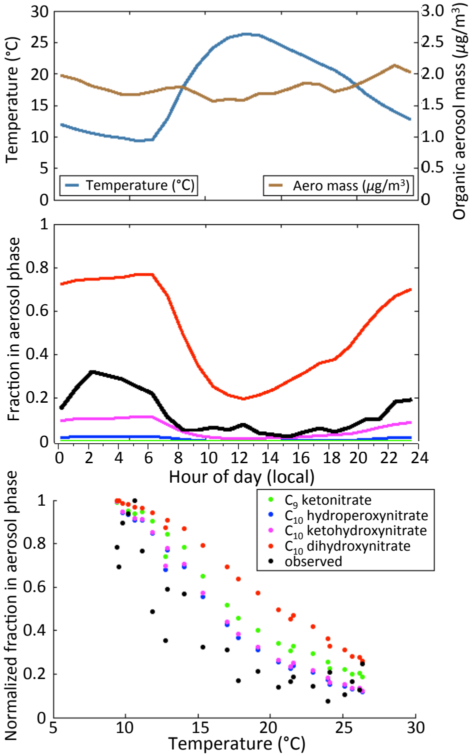

Fig. 9. Observed (black, same as in Fig. 5) and modeled fraction of organic nitrate in the aerosol phase over the diurnal cycle in temperature (blue) and background organic aerosol mass (measured by AMS, brown), based on calculated vapor pressures for a series of possible nitrate structures (indicated in legend). None of these structures can capture the observed dynamic range in aerosol fraction. Bottom panel shows aerosol fraction for the same series of molecules, demonstrating that the observed aerosol fraction does not fully scale with temperature as simple repartitioning of the same nitrates would predict. Data are normalized to peak fraction to facilitate comparison of the lineshapes.

Title Page
Abstract
Introduction
Conclusions
References
Tables
Figures
◀▌ ▐▶
◀ ▶
Back
Close
Full Screen / Esc
Printer-friendly Version
Interactive Discussion

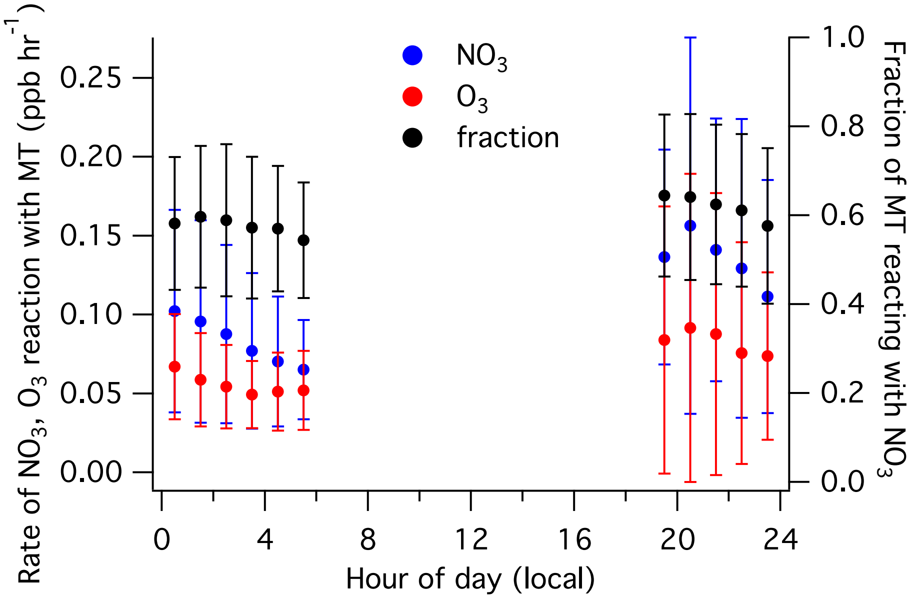

Fig. 10. Rates of reaction of NO_3 and O_3 with monoterpenes averaged for entire campaign, nighttime data only, using measured [O_3] and [monoterpenes], and using the production rate of NO_3 ($k_1[NO_2][O_3]$) to stand in for the rate of $NO_3 + MT$, since it is assumed that every NO_3 produced reacts with MT. Right axis: The fraction of total MT reactivity due to reactions with NO_3 (black) suggests a greater role for NO_3 than O_3 as the initial oxidant in nighttime oxidation.

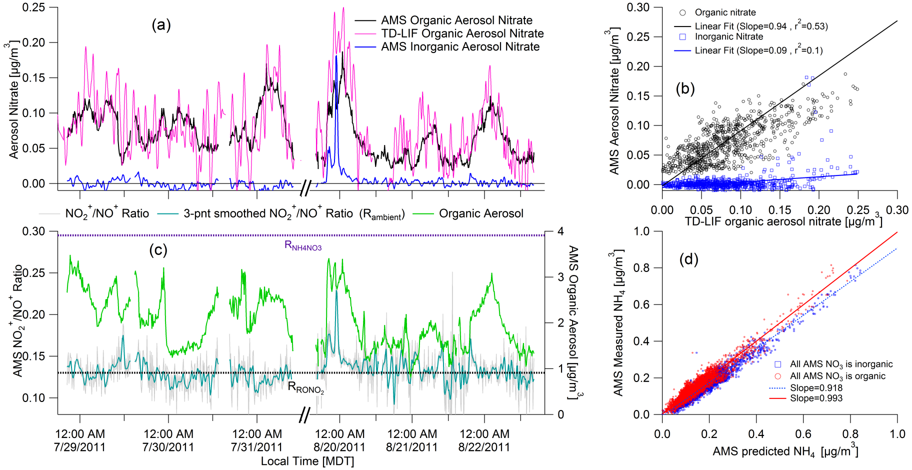

Fig. 11. **(a)** Concentration of AMS organic and inorganic nitrate, calculated based on the NO_2^+/NO^+ field ratios and $R_{RONO_2} = 0.13$, compared to aerosol organic nitrate measurements with the TD-LIF system, for the six days the ambient measurements of both instruments overlapped during RoMBAS. **(b)** Scatter plot of calculated AMS organic and inorganic nitrate with TD-LIF aerosol organic nitrate. **(c)** Total organic aerosol mass as measured by the AMS, and NO_2^+/NO^+ ($R_{ambient}$) used to calculate organic nitrate fraction in **(a)**. Also shown are the NO_2^+/NO^+ ratio determined in calibration with inorganic nitrate as well as the estimated R_{RONO_2} ratio. A 3-point smoothed version of the ratio was used when calculating $RONO_2$ **(d)** Cation vs. anion balance, evaluated by plotting measured AMS ammonium vs. predicted ammonium for two cases: assuming all AMS nitrate is inorganic and assuming it is all organic.

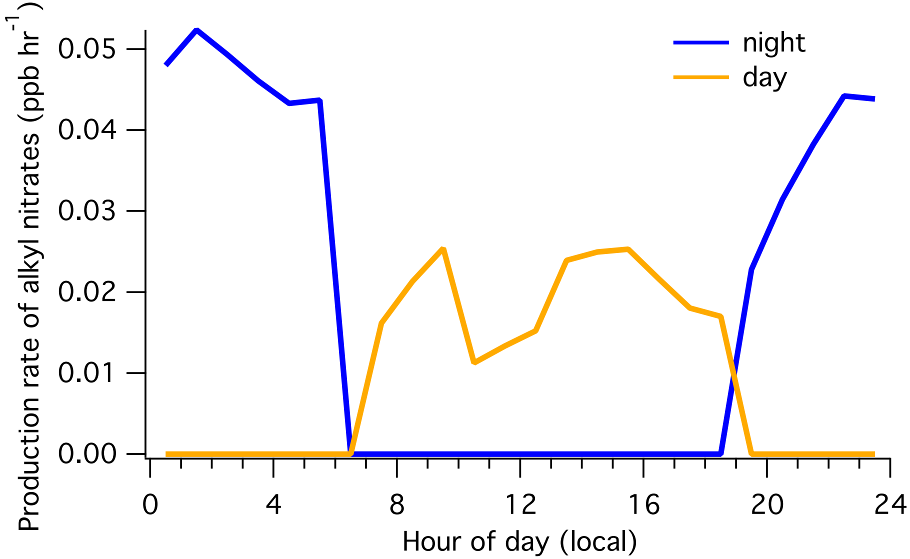

Fig. 12. Calculated rates of production of organic nitrates for daytime OH-initiated (yellow) and nighttime NO_3-initiated (blue) mechanisms. The fraction of RO_2 radicals that react with NO ranges from ≈ 40 %–90 % during the day (not shown).